J Mater Sci (2007) 42:266–297
DOI 10.1007/s10853-006-0842-9

Electrospray droplet sources for thin film deposition

A. Jaworek

Received: 23 August 2004 / Accepted: 17 October 2005 / Published online: 28 November 2006

Abstract Electrospraying utilises electrical forces for liquid atomisation. Droplets obtained by this method are highly charged to a fraction of the Rayleigh limit. The advantage of electrospraying is that the droplets can be extremely small, down to the order of 10's nanometres, and the charge and size of the droplets can be controlled to some extent be electrical means. Motion of the charged droplets can be controlled by electric field. The deposition efficiency of the charged spray on an object is usually higher than that for uncharged droplets. Electrospray is, or potentially can be applied to many processes in industry and in scientific instruments manufacturing. The paper reviews electrospray methods and devices, including liquid metal ion sources, used for thin film deposition. This technique is applied in modern material technologies, microelectronics, micromachining, and nanotechnology.

Introduction

Electrospraying is a method of liquid atomisation by electrical forces. The atomiser nozzle is usually made in the form of metal capillary, which is biased by a high voltage. The shear stress on the liquid surface, due to the established electric field, causes elongation of a jet and its disintegration into droplets. The droplets obtained by this method can be extremely small, in special cases down to nanometers. The advantage of the electrospray is that droplets are highly charged, up to a fraction of the Rayleigh limit. The Rayleigh limit [1] is the magnitude of charge on a drop, which overcomes the surface tension force that leads to the drop fission. This charge is given by the following equation:

$$Q_R = 2\pi(16\sigma_l\varepsilon_0 r^3)^{1/2} \tag{1}$$

in which σ_l is the liquid surface tension, ε_0 is the electric permittivity of the free space, and r is the droplet radius.

The charge and size of the droplets can be controlled to some extent by adjusting the liquid flow rate and the voltage applied to the nozzle. Charged droplets are self-dispersing in the space due to mutual Coulomb repulsion, that results in the absence of droplet's agglomeration. The expansion of a spherical cloud of charged droplets is given by the Eq. [2]:

$$-\frac{1}{c_\mathrm{d}}\frac{\mathrm{d}c_\mathrm{d}}{\mathrm{d}t} = \frac{2C_c\varepsilon_0 c_\mathrm{d}E_\mathrm{ds}^2}{\eta_\mathrm{g}\rho_\mathrm{l}} = \frac{c_\mathrm{d}}{\tau_\mathrm{exp}} \tag{2}$$

in which c_d is the initial mass concentration of the droplets, η_g is the gas dynamic viscosity, ρ_l is the liquid density, and C_c is the Cunningham slip correction factor.

E_ds is the electric field on a single droplet surface charged to the magnitude Q_d:

$$E_\mathrm{ds} = \frac{Q_\mathrm{d}}{4\pi\varepsilon_0 r^2} \tag{3}$$

In Eq. (2) τ_exp is time constant of the expansion of the cloud:

A. Jaworek (✉)
Institute of Fluid Flow Machinery,
Polish Academy of Sciences, Fiszera 14,
Gdańsk 80-952, Poland
e-mail: jaworek@imp.gda.pl

$$\tau_{\text{exp}} = \frac{\eta_{\text{g}}\rho_{\text{l}}}{2C_{\text{c}}\varepsilon_0 E_{\text{ds}}^2} \tag{4}$$

The mass concentration of the droplets due to the cloud expansion decreases reciprocally with time:

$$c_{\text{d}} = c_{\text{d0}}\left(1 - \frac{t}{\tau_{\text{exp}}}\right) \tag{5}$$

The motion of the charged droplets can be easily controlled (including deflection or focusing) by an electric field. The deposition of a charged spray or solid particles on an object can be more effective than for un-charged one [3]. An apparatus for electrospraying is very simple and cheap. Main shortcoming of electrospraying, limiting its widespread use in industry, is its low throughput. To overcome this problem, the multi-nozzle or slit-nozzle systems [4–11] were proposed. Mechanical spraying by rotary [12–14] or pneumatic atomisers [15–17] with grounded nozzle and high voltage induction electrode can also be used for production of large amount of charged spray. However, the charge of the droplets produced by this method is one order of magnitude lower than the Rayleigh limit.

One of the most important features characterising any spray system is the mode of spraying. There were many spraying modes discovered and discussed in the literature [18–25], but they can be categorised into two main groups:

- The first group, which is characteristic in that only fragments of liquid are ejected directly from the meniscus at the capillary outlet. These fragments can be in the form of regular large drops, fine droplets, or elongated spindles at the moment of their detachment.
- In the second group, the liquid is elongated into a fine jet, which disintegrates into droplets due to its instability. It was observed that the jet could be smooth and stable or could move in a regular way: rotate around the capillary axis or oscillate in its plane [22]. Sometimes a few jets on the circumference of the capillary can be formed.

Charged sprays found application in many fields, including painting or thin film deposition. The physical and chemical methods for thin and thick films deposition from gaseous, solution, molten or solid state were reviewed by Altenburg et al. [26] but only minor attention was devoted to the electrospraying. Recently, Choy [27] reviewed of the current and potential development of chemical vapour deposition processes and their application to film deposition, with only brief presentation of electrospraying. Therefore, there is a need for presentation of electrospray applications in the thin film technology with a summary of the benefits it offers in this field.

The purpose of this paper is to outline electrospray devices, including liquid metal ion sources, used for thin solid film deposition. The advantages that electrospray has over other methods of metal or ceramic film production are also pointed out. All the relevant details of the available technical data regarding fundamental experiments and laboratory demonstrations on the electrostatic method of thin film deposition are summarised in the tables.

Thin solid film deposition

Introduction

Thin solid films are used to improve surface properties of mechanical elements or in scientific or measuring instruments, and in electronic devices. Electrostatic deposition is the process of depositing a material on a substrate by electrical forces. Initially, electrospray was used to produce thin layers of radioactive materials, such as α- or β particle sources, or targets prepared for activation in particle accelerators or nuclear reactors. Recently, electrospray was used for thin film deposition in nanotechnology and nanoelectronics.

There are several methods used for thin layer deposition on a substrate:

1. casting of a solution or colloid suspension on a substrate, followed by solvent evaporation,
2. cathode spraying, applicable for metal layers preparation,
3. condensation of vapours of a material on the substrate,
4. radio-frequency sputtering,
5. laser ablation,
6. chemical vapour deposition,
7. physical vapour deposition,
8. microwave plasma coating,
9. flame-assisted vapour deposition,
10. electrodeposition of the layer by electrolysis, used for metals deposition,
11. electrospraying.

Large amount of material is lost to the chamber walls when cathode spraying, chemical vapour deposition, or vapour condensation is used. When a solution or suspension of a material to be deposited is sprayed

by mechanical atomisers, or simply poured onto a substrate, the layer is not sufficiently homogeneous and of the same thickness on the entire surface.

The quality of thin film formed on a substrate strongly depends on the size of particles or droplets forming the layer, their monodispersity, and their uniform distribution on the surface. Smaller particles, of narrow size distribution should be generated in order to reduce the number and size of voids, flaws and cracks in the film. The droplets ought to be uniformly dispersed over the substrate to ensure the layer to be even and of the same thickness. The electrospray is a promising tool for production of high quality layers and films because it fulfils all these requirements. The electrostatic technique allows generating fine droplets in micro- and submicrometer size range, with narrow size distribution. Electrostatic forces disperse the droplets homogeneously in the space between the nozzle and the substrate. The electrospray process is also easy to control by adjusting liquid flow rate and the voltage applied to the nozzle, and it is less expensive in production of thin films than chemical or physical vapour deposition, or plasma spraying requiring high vacuum installations. The film thickness can be simple controlled by varying the concentration and flow rate of the precursor solution.

There are two main spray systems used for thin film deposition:

1. simple nozzle facing directly the substrate; high voltage is applied either to the nozzle or the substrate, while the counter electrode is grounded (Fig. 1a),
2. nozzle–extractor system, which operates independently of the substrate; the nozzle is at high potential while the extractor and the substrate are grounded (Fig. 1b).

A disadvantage of the first system is that the substrate is one of the active electrodes, and should be conducting. If an electric current to the substrate is not allowed, because the substrate could be damaged, the second spray system, with an extractor electrode, is used. However, a disadvantage of this system is that a fraction of the total number of droplets is deposited on the extractor electrode, and special precautions are needed to prevent these droplets to fall onto the substrate. Reverse configuration, with the substrate placed above the nozzle outlet, which now is facing upwards, or systems with horizontal nozzle were therefore used by van Zomeren et al. [28], Chen et al. [29–31], Lapham et al. [32], Taniguchi et al. [33, 34], and Perednis et al. [35]. In these systems, only sufficiently fine droplets are accelerated by the electric field and reach the substrate.

In order to improve operational properties of electrospray devices also other modifications were proposed. A guard electrode was used to obtain more uniform electric field in the interelectrode space by Jaworek and Krupa [22, 23] (Fig. 2a). With the guard plate, the electrospray is more stable, the spray plume angle is narrower, and the system operates in wider voltage range [36]. Kim et al. [37, 38] applied a pyrex guide tube placed between the nozzle and the substrate, which focused the droplets on the substrate surface (Fig. 2b). A heated sheath gas was pumped through this tube for solvent evaporation. The film obtained was more uniform when using this device. Sorensen [39] designed a 'trumpet-ended' nozzle made of stainless steel capillary with central sharp electrode (Fig. 3). The spray plume was wider because the liquid was sprayed both from the electrode tip and the edge of the 'trumpet'. Tilted nozzles (ended like a hypodermic needle) were also tested as a source of droplets. Chen [31] argued that such nozzle allow the cone-jet mode to operate in wider voltage and flow rate ranges. Recently, Li [40] proposed a nozzle with a concentric dielectric fibre protruding from the nozzle at some distance. Such insulating fibre is not an ion injector, and does not affect the spraying by electrical but only by capillary forces.

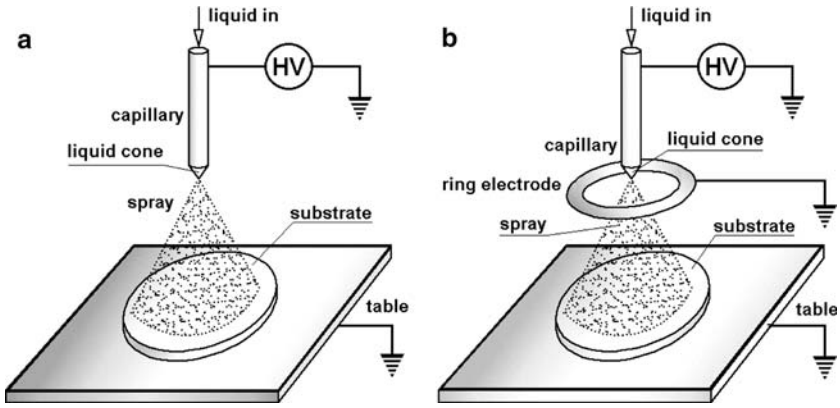

Fig. 1 Thin film deposition by liquid atomisation, (**a**) simple nozzle for direct spraying, (**b**) nozzle–extractor system

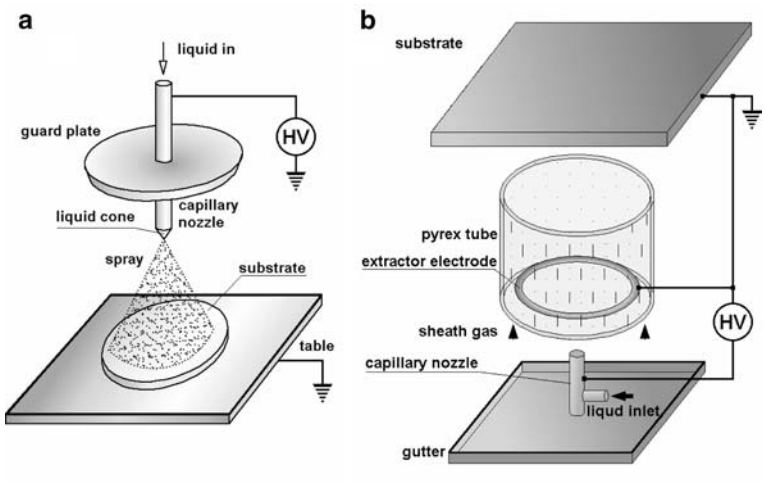

Fig. 2 Spray systems (**a**) with guard plate, (**b**) with pyrex guide tube and sheath gas

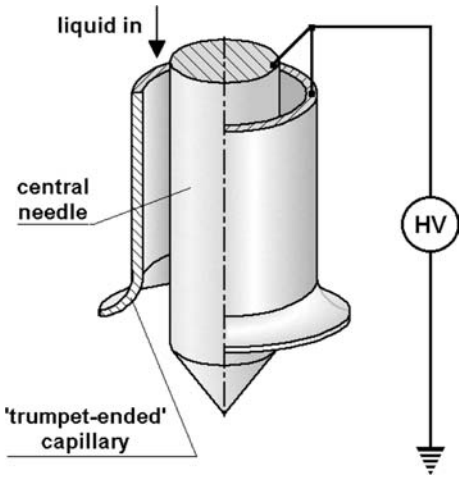

Fig. 3 Schematic diagram of the 'trumpet ended' spray nozzle for thin film deposition [cf. 39]

Depositing droplets on an insulating surface presents serious problems due to charge accumulation, repelling on-coming droplets. Kessick et al. [41], solved this problem by using ac potential for electrospraying. Ac potential was capable of producing high quality coverage due to reduction of the net charge on the surface.

Thin film deposition technique using electrospray for thin film deposition is frequently called 'electrostatic spray deposition' (ESD), 'electrostatic spray assisted vapour deposition' (ESAVD) [42], or 'electrostatic spray pyrolysis' (ESP) when the process proceeds at high temperatures. The spray systems usually operate in the cone-jet mode but, sometimes, the multi-jet mode also is used [37, 38]. The multi-jet mode made it possible to obtain simultaneously a large number of emission cones and droplets smaller than from a single cone. The details of the experiments with thin film deposition by electrospraying are briefly summarised in Table 1.

The process of depositing a layer from a liquid phase of an on-demand structure or pattern is called 'direct writing'. The advantage of such technology is that the patterns are printed directly onto a substrate under computer control without a need of using photolithographic masks, and that the layer needs not to be patterned after deposition. Electrospray technique was also tested for these processes. Direct write techniques are capable of producing structures with feature sizes smaller than 100 μm and in near future it is expected to decrease this limit to 10's μm [129].

Usually, the material to be deposited is sprayed directly onto the substrate. However, the layer can also be obtained from other compounds, known as precursors. The precursors can be decomposed at a high temperature or react with other compounds sprayed simultaneously. The decomposition and reactions can be carried out on the heated substrate, or in a heated gas, in the way of a droplet to the substrate. In the latest case, only the reaction products are deposited on the surface.

The electrostatic spray deposition processes are carried out at lower temperatures than conventional solid-state reactions. The optimum temperature of the substrate is critical for this process, for layer uniformity and porosity. The porosity is a result of fast evaporation of the solvent, and increases with the substrate temperature. Changing the composition of the solvent by addition of a liquid of higher boiling temperature can help in control the evaporation process. When, for example, butyl carbitol was added to ethanol, used as the solvent, the film structure was more uniform [61].

Surface morphology, chemistry, and crystal structure are usually studied using scanning electron microscopy (SEM), energy-dispersion X-ray microanalysis

Table 1 Thin film deposition – Comparison of methods and results

Authors	Application (layer// substrate)	Substance or precursor sprayed	Solvent	Nozzle	Voltage (electrode distance)	Flow rate (growth rate or deposition time)	Spray current (specific charge)	Film thickness (plume base diameter)
Carswell and Milsted [43]	α-sources (nuclear cross section studies)	Nitrates of Am^{241}, Cm^{242}, U^{233}, Pu^{238}	Acetone	Glass capillary 0.2 mm o.d., concentric wire	4–6 kV (10–20 mm)	30 μl/h	0.1–0.2 μA	40 μg/cm^2
Gorodinsky [44]	Source of radioactive radiation	Ruthenium salts or uranium nitrate	Ethanol + water mixture	Glass capillary 0.1–0.3 mm, Pt wire 0.05 mm	7–8 kV (10–50 mm)		0.1–0.5 μA	1–2 μg/cm^2 (20–30 mm)
Bruninx and Rudstam [45]	Samples for β counting	Nb^{95} + CsI, Cs^{137} + CsI, Cs^{137} + ZnBr, Cs^{137} + Methylene blue, Ru^{106} + CsI	Acetone, ethyl ether, ethyl acetate, ethanol, methanol, *n*-butyl alcohol	Glass capillary 0.1–0.5 mm, stainless steel or Pt wire	1–10 kV (7 mm)	(500 μg)	0.1–0.5 μA	50–450 μg/cm^2
Lauer and Verdingh [46]	Nuclear cross section measurements, neutron detectors	Uranium acetate, plutonium acetate, boric acid (H_3BO_3)	Methyl alcohol	Stainless steel capillary 0.05–0.08 mm i.d.	< 13 kV			< 10 mg/cm^2
Michelson [47], Shorey and Michelson [48]	Nuclear spectroscopy, neutron cross-section studies	NaCl	Ethanol, methanol, isopropanol, isobutanol, *n*-butanol, amyl alcohol, formic acid	Pyrex tube	3–8 kV (10 mm)		0.3–0.6 μA	0.2 μm crystallites
Teer and Dole [49]	Thin film, (polystyrene latex // Al foil)	Polystyrene latex	Toluene, acetone + benzene, acetone + cyclohexane	Stainless steel capillary 0.2 mm i.d., 0.41 mm o.d.	9–24 kV (220 mm)	4.8 mL/h		
Mahoney and Perel [50]	Solar cells	Molten Si (1500°C)			10 kV		500 μA	
Pang et al. [51]	Solar cells	Molten Si (1420°C)			10 kV		500 μA	
Hall and Hemming [52]	Photosensitive resists			Centrifugal spraying, induction charging				20–30 μm
Thundat et al. [53]	Samples for scanning tunnelling microscopy	DNA		Glass capillary 0.8 mm o.d., pulled to μm size, Pt wire	1.5 kV (5 mm)	(2–6 s)		(5 mm)
van Zomeren et al. [28]	Cathodes for lithium batteries	$Mn(CH_3COO)_2 \cdot 4H_2O$ + LiCl	Ethanol	Stainless steel capillary 0.8 mm i.d.	8–20 kV (neg.) (5–30 mm)	(1–5 μm/h growth rate)	< 50 μA	300 nm crystallites, (4 μm droplets)
Ryu and Kim [54]	Electronic devices (ZnO // Si) (340–400 °C)	Zinc trifluoroacetate	Methanol	Glass capillary with tungsten needle	< 20 kV			20 nm crystallites
Chen et al. [29, 30, 55, 56]	Lithium batteries ($LiCoO_2$ // ITO glass or stainless steel or Al) (230–450 °C)	0.04 M $Co(NO_3)_2 \cdot 6H_2O$ + 0.04M $Li(CH_3COO) \cdot 2H_2O$	Ethanol or ethanol (15% vol.) + butyl carbitol (85%)	Stainless steel capillary	8–12.5 kV (20–60 mm)	2 mL/h (120 min)		
Chen et al. [57]	Solid electrolyte for fuel cells (250–430 °C)	Ziconia stabilised by yttria	ethanol + butyl carbitol		8–10 kV (30 mm)			15 μm
Denisyuk [58]	Optical layers	Plastic materials	Dimethyl formamide, toluene, xylene, butyl acetate, ethyl acetate	Plastic capillary 0.5 mm i.d. with metal needle	20 kV		1–10 μA	1.5–5 μm

Table 1 continued

Authors	Application (layer// substrate)	Substance or precursor sprayed	Solvent	Nozzle	Voltage (electrode distance)	Flow rate (growth rate or deposition time)	Spray current (specific charge)	Film thickness (plume base diameter)
Hoyer et al. [59]	Membranes for analytical chemistry	Cellulose acetate	Acetone with magnesium perchlorate additive	Stainless steel capillary 0.14 mm i.d. 0.3 mm o.d.	14 kV (35 mm)	1.08 mL/h	1–11 μA	300 nm (3.8 mm)
Stelzer and Schoonman [60]	Fuel cells (terbia-doped yttria-stabilised zirconia // nickel, or stainless steel) (250–500 °C)	Yttrium- and zirconium-acetylacetonate and terbium-acetate hydrate	Ethanol + butyl carbitol (50:50% vol., or 20:80% vol.)					
Chen et al. [61]	Lithium batteries, ($Li_xMn_2O_4$ – as cathode and Li_xBPO_4 – as solid electrolyte/Al or stainless steel) (250 °C)	0.005 M $Li(CH_3COO) \cdot 2H_2O$ + $Mn(CH_3COO)_2 \cdot 4H_2O$ + H_3BO_4 + P_2O_5	ethanol or ethanol + butyl carbitol (+ acetic acid)		8–12 kV (20–30 mm)			
Sobota and Sorensen [62]; Sorensen [39]	Solid lubricating films (MoS_2 // silicon)	MoS_2 (120 × 1000 μm platelets)	Isopropanol, Acetone, alcohol or toluene	Annular-slit nozzle 10 μm gap, stainless steel capillary 0.9 mm i.d. 1.2 mm o.d.	3–20 kV (180 mm to substrate)	2.4 mL/h (25 min)	(0.5–2.5 mA/cm^2)	0.28–1 μm
Teng et al. [63]	Ceramic films, membranes, (ZrO_2 // silicone release paper)	ZrO_2, (0.2 μm suspension)	Butyl acetate + ethanol	Stainless steel capillary 0.26 mm i.d. 0.51 mm o.d.	3–10 kV (8 mm to extractor ring of 10 mm dia.)	0.6–45 mL/h (0.2 g/h deposition rate)		< 10 μm droplets: (2–15 μm donut-like relics)
Chen et al. [64]	Optoelectronic devices (TiO_2), lithium batteries ($LiMn_2O_4$ // Al, Pt or ITO glass) (250 °C)	0.005M $Ti(i\text{-}C_3H_7O)_4$, 0.005M $Li(CH_3COO) \cdot 2H_2O$ + 0.01M $Mn(CH_3COO)_2 \cdot 4H_2O$	Ethanol or ethanol + butyl carbitol (+ acetic acid)		10 kV	1.2 mL/h		1 μm particles
Choy et al. [65]	Fuel cells, multilayer ($La(Sr)MnO_3$ // Zr $(Y)O_x$ // Ni-ZrO_2) (400–550 °C)					1.2 mL/h (60–300 μm/h growth rate)		5–20 μm
Cich et al. [66]	Plasma display panels of $(Zn,Mn)_2SiO_2$ // Si(111))	$Mn(CH_3COO)_2$ + $Zn(CH_3COO)_2$ + tetraethyl orthosilicate	Ethanol		11–17 kV	0.75–4.5 mL/h		0.75–1 μm
Gourari et al. [67, 68]	H_2 gas sensors, (SnO_2 or SnO_2:Mn_2O_3 // Al or alumina pellets) (400 °C)	0.01–0.1M $SnCl_4 \cdot 5H_2O$ + $Mn(CH_3COO)_2 \cdot 4H_2O$	Ethanol		10 kV	1.2–9.3 mL/h		1–10 μm grains
Heine et al. [69]	Quantum dots for photo-luminescence (ZnS coated CdSe // glass) (1–4 mg/CdSe/mL) (100–300 °C)	CdSe (in ZnS matrix)	Acetonitrile + pyridine (2:1)		3.7–4 kV	0.6–1.8 mL/h		0.5–1 μm (20–40 nm grains with 2.8 nm CdSe nanocrystals)

Table 1 continued

Authors	Application (layer// substrate)	Substance or precursor sprayed	Solvent	Nozzle	Voltage (electrode distance)	Flow rate (growth rate or deposition time)	Spray current (specific charge)	Film thickness (plume base diameter)
Nishizawa et al. [70]	Lithium batteries ($LiMn_2O_4$ // Pt film // SiO_2 // Si) (400 °C)	0.025 M $LiNO_3$ + 0.05M $Mn(NO_3)_2$	Ethanol	Stainless steel capillary 0.8 mm i.d	12 kV (25 mm)	2 mL/h (30 min)		0.5 μm
Chen et al. [31]	Ceramic films (ZnO, ZrO_2, Al_2O_3, CoO // Al) (100–250 °C)	0.05M $Co(NO_3)_2 \cdot 6H_2O$, or $SnCl_4 \cdot 5H_20$ + $Zn(CH_3COO)_2 \cdot 2H_2O$	Ethanol + butyl carbitol or ethanol	Stainless steel capillary 0.4 mm i.d. 0.6 mm o.d. or 0.6 mm i.d. 0.8 mm o.d. (flat or tilted)	8.8 kV (20 mm)	0.8 mL/h or 1.5 mL/h (60 min)		100 nm (particle size)
Chen et al. [71]	Solar cells (TiO_2 // Al, Pt or ITO glass) (100–220 °C)	0.01M $Ti(OCH(CH_3)_2)_4$	Ethanol		8–15 kV (30 mm)	0.08 mL/h		1 μm particles (20–30 nm crystallites)
Choy and Su [42]	Optoelectronic devices, solar cells (TiO_2 // SnO_2 coated glass) (350–550 °C)	Titanium diisopropoxide bis(2,4-pentamedionate	2-propanol			(20 min)		0.5 μm (10–60 nm crystallites)
Miao et al. [72–75], Balachandran et al. [76]	Ceramic films, membranes, (ZrO_2, SiC // Si or CrFe alloy)	ZrO_2, SiC (suspension)	Ethanol + water mixture (1:1 by vol.)	Stainless steel capillary 0.23 mm i.d. 0.51 mm o.d.	4–8 kV (8 mm to extractor ring of 15 mm dia.)	0.4–1.8 mL/h (2 min)	0.2 μA (ZrO_2) 0.12 μA (SiC) 0.61 C/kg (ZrO_2) 0.31 C/kg (SiC)	< 10 μm droplets: (4–8 μm ZrO_2) (3.5–5.5 μm SiC)
Moerman et al. [77]	Chemical analysis by fluorescence detection	Rhodamine	Glycol + water mixture (0.7/0.3 by volume)	0.1 mm i.d. 0.2 mm o.d.	1.2 kV (0.3–0.4 mm)	0.072 nl/h – 1.08 mL/h		(200 μm dots)
Su and Choy [78]	(SiO_2 // glass or Si wafer) (80–120 °C)	Silica sol in H_2O (0.2–1 gSiO_2/l) 13 μm particles	Ethanol		(3–8 kV/cm)	5–10 mL/h		
Turetsky [79]	Semiconductor films (CdS, ZnS)	CdS, ZnS	Water-ethanol mixture		3–8 kV			1–100 μm (monodisperse droplets)
Yamada et al. [80]	Lithium batteries, ($LiNiO_2$, or $LiCo_{0.5}Ni_{0.5}O_2$, or $LiAl_{0.25}Ni_{0.75}O_2$ // Au) (450 °C)	0.025M $Li(CH_3COO) \cdot 2H_2O$ + $Ni(CH_3COO)_2 \cdot 4H_2O$ + {$Co(NO_3)_2 \cdot 6H_2O$ or $Al(NO_3)_3 \cdot 9H_2O$}		Stainless steel capillary 0.3 mm i.d 0.5 mm o.d	11 kV (55 mm)	3.9 mL/h (60–360 min) (1.6 μm/h growth rate)		1.6–10.3 μm ($LiNiO_2$)
Kim et al. [37, 38]	Plasma displays, (MgO // glass or SiO_2/Si) (400–500 °C)	$Mg(C_{11}H_{19}O_2)_2$	Ethanol (90%) + acetic acid (10%) or tetrahydrofuran + 1-butyl alcohol	Stainless steel capillary 0.4 mm i.d. 0.7 mm o.d.	13 kV (glass) 14.5 kV (SiO_2/Si) (55 mm to ring extractor)	7.6 mL/h (glass) 16 mL/h (SiO_2/Si) (0.2–0.53 μm/h growth rate) (60 min)		0.5 μm (0.1–0.5 μm particle size)
Reifarth et al. [81]	Neutron detectors (^{34}S // Al)	^{34}S (94.3% purity)	Toluene		9 kV (10 mm)			0.5–2.2 mg/cm^2

Table 1 continued

Authors	Application (layer// substrate)	Substance or precursor sprayed	Solvent	Nozzle	Voltage (electrode distance)	Flow rate (growth rate or deposition time)	Spray current (specific charge)	Film thickness (plume base diameter)
Su and Choy [82, 83]; Choy and Su [84]; Su et al. [85]	Optoelectronic devices, solar cells, (CdSe or CdS // ITO coated glass) (200–450 °C)	0.005 M $CdCl_2$ + $(NH_2)_2CSe$ or 0.005M $CdCl_2$ + $(NH_2)_2CS$	Ethanol + water	Ultrasonic nebuliser (1.7 MHz)	5–10 kV (CdSe) 4–20 kV (CdS)	10–30 mL/h (2–5 min CdSe) (10–60 min CdS) (3 μm/h growth rate)		10–35 nm (CdS crystallites size) (100–200 nm CdSe grain size) (80–200 nm CdS grain size)
Zaouk et al. [86, 87]	Optoelectronic devices, (SnO_2:F // glass) (500–550 °C)	0.25 M $SnCl_4 \cdot 5H_2O$ + 0.2M HF	Ethanol		10.5 kV (60 mm)	13.2 mL/h (1.44 μm/h growth rate)		
Chandrasekhar and Choy [88]; Raj and Choy [89]	ITO films, (Sn:In_2O_3 // glass) (200–550 °C)	0.05 M tin tetrachloride + indium chloride	Ethanol		5–20 kV	(5–45 min)		0.5 μm (15–55 nm crystallites, 250–600 nm grains)
Chandrasekhar and Choy [90]	Optoelectronic devices, solar cells (SnO_2:F // glass) (350–600 °C)	0.05 M $Sn(CH_3COO)$ + hydrofluoric acid	Methanol		5–15 kV (20–50 mm)	20–40 mL/h (60 min)		0.5 μm (250–400 nm grain size)
Choy [91]; Wei and Choy [92]	Light emitting diodes (ZnS // glass or Si(100)) (450–550 °C)	0.01 M $ZnCl_2$ + $(NH_2)_2CS$	water		4–25 kV	10–30 mL/h (6 μm/h deposition rate)		(20 nm crystallites at 450°C); (80–200 nm crystallites at 500°C)
Diagne and Lumbreras [93]	CO_2 gas sensors, (SnO_2 + LaOCl // Si wafer or Al pellets) (400 °C)	0.1 M $SnCl_4 \cdot 5H_2O$ + $LaCl_3 \cdot 6H_2O$	ethanol		10 kV (30 mm)	0.7 mL/h		10–25 μm grains
Lapham et al. [32]	Electrocatalyst, ($NiCo_2O_4$ // alumina particles) (350–400 °C)	0.05 M $Ni(NO_3)_2 \cdot 6H_2O$ + $Co(NO_3)_2 \cdot 6H_2O$	Ethanol (20% vol.) + di(ethylene glycol) butyl ether (80%)		(30 mm)	0.55 mL/h (120 min)		62 μm 0.5 μm (particles)
Moerman et al. [94, 95]	Biologically active micrometer spots (50 nm silicone nitride // Si wafer)	Enzymes, antibodies, rhodamine	Water, ethylene glycol + water mixture	Stainless steel capillary 0.06 mm i.d., 0.16 mm o.d.	0.95–1.8 kV (0.22–0.4 mm)	0.36–4 μl/h	0.5 μA	(130–315 μm spots)
Mohamedi et al. [96]	Anodes for lithium batteries, (SnO_2 // Ni) (400 °C)	0.05 M $SnCl_4 \cdot 5H_2O$	Ethanol	Stainless steel capillary 0.8 mm i.d.	12 kV (25 or 40 mm)	2 mL/h (30 min)		1 μm (particles)
Mohamedi et al. [97–99]	Lithium batteries, ($LiMn_2O_4$ // Au) (400°C)	0.025 M $LiNO_3$ + 0.05M $Mn(NO_3)_2$	Ethanol	Stainless steel capillary 0.8 mm i.d.	12 kV (25 mm)	2 mL/h (3–30 min)		0.1–1 μm
Nguyen and Djurado [100]	Fuel cells, (ZrO_2:Y_2O_3 // stainless steel) (300–400 °C)	0.05 M zirconium acetylacetonate + 0.05M yttrium acetylacetonate	Ethanol (14% vol.) + butyl carbitol (56%) + acetic acid (30%)		14–20 kV (30 mm)	2–3.9 mL/h (6–120 min)		0.5 μm (amorphous) (7.8 nm crystallites for 3.9 mL/h)

Table 1 continued

Authors	Application (layer// substrate)	Substance or precursor sprayed	Solvent	Nozzle	Voltage (electrode distance)	Flow rate (growth rate or deposition time)	Spray current (specific charge)	Film thickness (plume base diameter)
Rhee et al. [101]	Buffer layer for superconductors or ferroelectric films (MgO // Si) (265–400 °C)	0.1 or 0.2 M $Mg(CH_3COO)_2$	Ethanol		10–17 kV (50 mm)	0.36–3.6 mL/h (4 μm/h growth rate)	(1/3 of Rayleigh limit)	0.3–1 μm (5–20 nm roughness)
Yoon et al. [102]	Lithium batteries, ($LiCoO_2$ //Pt coated alumina) (300 °C)	0.04 M $LiNO_3$ + 0.04M $Co(NO_3)_2{\cdot}6H_2O$	Ethanol		10–15 kV (40 mm)	2 mL/h (15–120 min) (0.67 μm/h growth rate)		0.1–0.7 mg/cm^2
Cao and Prakash [103]	Lithium batteries, ($LiMn_2O_3$ // Al or SnO_2 coated glass) (300°C)	0.006 M $Mg(CH_3COO)_2{\cdot}4H_2O$ + 0.003 M $Li(CH_3COO)_2{\cdot}2H_2O$			10 kV (30 mm)	2 mL/h		10 μm
Jayasinghe et al. [104,105]; Jayasinghe and Edirisinghe [106–108]	Ceramic films (reprographic technique for microengineering) ceramic foam	Alumina (20% by vol) (0.5 μm particles)	Ethanol	Stainless steel capillary 0.2 mm i.d., 0.48 mm o.d.	5–12 kV (6 or 8 mm to extractor)	0.3 or 6 mL/h (1 h spray time for foam production)	0.053–0.059 μA	(30–60 μm droplets relics)
Kobayashi et al. [109]	Lithium batteries ($LiMn_2O_4$ // $(Li,La)TiO_3$) (400 °C)	0.03 M $LiNO_3$ + 0.05M $Mn(NO_3)_2{\cdot}6H_2O$	Ethanol	Stainless steel capillary, 0.5 mm i.d.	9 kV (25 mm)	2 mL/h		(40 mm)
Dokko et al. [110, 111]	Lithium batteries, ($LiCo_xMn_{2-x}O_4$ // Au)	0.025M $LiNO_3$ + 0.05M $\{Co(NO_3)_2$ + $Mn(NO_3)_2\}$	Ethanol		12 kV	(15 min)		0.5 μm
Huang et al. [112]	Dynamic RAM, piezoelectronic devices ($PbTiO_3$ // *n*-Si) (150 °C)	$Pb(OAc)_2{\cdot}3H_2O$ + $[CH_3(CH_2)_3O]_4Ti$	2-ethoxy ethanol	Quartz tube 0.4 mm	12 kV (25 mm)	2.7 mL/h (20–40 min)		0.35 μm (45 nm grains)
Kim et al. [113]	Lithium batteries (V_2O_5 // Pt) (200 °C)	0.05M $[(CH_3)_2CHO]_3VO$	Ethanol		(40 mm)	2 mL/h (60 min)		
Lu et al. [114]	Piezoelectric microactuator for MEMS ($Pb(Zr, Ti)O_3$ // SiO_2 // Si) (25 or 100 °C)	$Zr(C_3H_7O)_4$+ $Ti((CH_3)_2CHO)_4$ + $P(CH_3COO)_2$			4.5 kV	0.6 mL/h		2 μm (150–200 nm crystallites)
Taniguchi et al. [33, 34]	Fuel cells ($Gd_xCe_{1-x}O_2$ or $La_{1-x}Sr_xCo_{1-y}Fe_y\ O_3$ // stainless steel or GdCeO pellets) (230–350 °C)	$Gd(NO_3)_3{\cdot}6H_2O$ + $Ce(NO_3)_3{\cdot}6H_2O$ or $La(NO_3)_3{\cdot}6H_2O$ + $Ga(NO_3)_2{\cdot}5H_2O$ + $SrCl_2{\bullet}6H_2O$ + $Mg(NO_3)_2{\cdot}6H_2O$	Ethanol + butyl carbitol (0.2/0.8 or 0.33/0.67 by volume)	Stainless steel capillary 0.4 mm i.d. 0.6 mm o.d.	4.1–5.5 kV or 5.9–6.5 kV (15 mm)	0.5–2.5 mL/h (15–240 min)		(14.9 mm)
Shu et al. [115, 116]; Chung et al. [117]	Lithium batteries ($LiMn_2O_4$ // Pt coated quartz)	0.025M $Li(CH_3COO){\cdot}2H_2O$ + 0.05M $Mn(NO_3)_2{\cdot}4H_2O$	Ethanol	Stainless steel capillary		2 mL/h (60 min)		11.9 μg/cm^2; 0.7–1 μm

Table 1 continued

Authors	Application (layer// substrate)	Substance or precursor sprayed	Solvent	Nozzle	Voltage (electrode distance)	Flow rate (growth rate or deposition time)	Spray current (specific charge)	Film thickness (plume base diameter)
How and Choy [118]	Anticorrosion film, (TiO_2 // glass, or stainless steel) (300–600°C)	0.05–0.5 M titanium diisopropoxide bis(2,4-pentamedionate	2-propanol					4 μm (200–500 nm grains)
Jayasinghe et al. [119]	Ceramic films, electrostatic printing (SiO_2 //quartz glass)	Silica (17% by vol.) (20 nm particles)	Ethylene glycol	Stainless steel capillary 0.2 mm i.d., 0.5 mm o.d.	10 kV (10 mm to ring extractor)	36 mL/h		(0.5–20 μm droplets, 1–80 μm droplets relics)
Kessick et al. [41]	(Carboxymethylcellulose // Si or polycarbonate)	Carboxymethyl-cellulose (0.01% solution)	MeOH + water (0.5/0.5 by vol.)	Glass capillary 0.02 mm i.d.	5–7.5 kVac/ 60 Hz (30 mm)	0.12 mL/h		
Kim et al. [120]	Capacitors (RuO // Pt // Si or RuO // Pt // quartz) (200°C)	$RuCl_3{\cdot}xH_2O$	Ethanol + butyl carbitol (0.2/0.8 by volume)					13 μg/cm^2
Matsushima et al. [121]	Gas sensors (SnO_2 // pyrex glass substrate)	$SnCl_2$ (500 °C)	Ethanol		10 kV (50 mm)	1 mL/h (30–180 min) (0.4 μm/h growth rate)		0.2–1 μm (30–160 nm particle size)
Morota et al. [122]	(Poly(ethylene oxide) // Al) (25 °C)	Poly(ethylene oxide) 50–70 g/L	Water + (ethanol or methanol or 1-propanol) + hexanol + $CaCl_2$	Glass capillary 0.05 mm tip, Pt 1.15 mm ion injector	3–7 kV (70 mm)	0.017–0.63 μl/h (1 min)	0.3–0.4 mA	
Saf et al. [123]	Electrostatic printing (polymer // ITO // glass)	Oligo(methyl-methacrilate) n = 9 polymerisation degree	Acetone (94% by vol.) + THF (5%) + water (1%)	Stainless steel capillary	2.7 kV (to extractor cylinder), 5.1 kV (to grounded substrate)	0.18 mL/h (0.08–0.15 μg/min growth rate)		30–130 nm (1.3 nm roughness), 0.1 mm spot
Sanders et al. [124]	Fuel cells (Nafion // PTFE)	Nafion (5% by wt.)	Aliphatic alcohol + water		20 kV (70 mm)	2 mL/h		50–60 μm
Siebers et al. [125]; Leeuwenbourgh et al. [126]	Endosseous implants (CaP coating // $TiAl_6V_4$ alloy) (300 °C)	0.0031 M $Ca(NO_3)_2{\cdot}4H_2O$ + 0.0019M H_3PO_4	Ethanol or butyl carbitol	Stainless steel capillary 1.0 mm i.d 1.4 mm o.d.	5.5–8 kV (15 or 20 mm)	1 or 2 mL/h (60 min)		0.5–2 μm
Uematsu et al. [127]	Biotechnology (α-lactalbumina // Al // poly(ethylene terephthalate)) (25 °C)	α-lactalbumina (0.4–1.8 μg/mL)	Water	Glass capillary 0.05 mm tip, Pt 1.15 mm ion injector	3.5 kV (30–40 mm) (ion collimator at 100 V to substrate)	(10 min)		300–700 μm
Jayasinghe and Edirisinghe [128]	Electrostatic printing (alumina // polyester)	Alumina (21% by vol.) (500 nm particles)	Ethanol	Stainless steel capillary 0.2 mm i.d., 0.48 mm o.d.	5–13 kV (6 mm to counter needle)	0.0036–0.036 mL/h		(1–35 μm relics, 4–8 μm mean)
Perednis et al. [35]	Fuel cells (ZrO_2:Y_2O_3 // $Ni_{72}Cr_{16}Fe_8$ – substrate disk 35 mm dia., 75 μm thick) (185–350°C)	0.17 or 0.085 M $Zr(C_5H_7O_2)_4$ or $Zr(C_3H_7O)_4$ or $ZrO(NO_3)_2{\cdot}xH_2O$ or $ZrCl_4$ + 0.03 or 0.015 M $YCl_3{\cdot}6H_2O$ or $Y(NO_3)_3{\cdot}6H_2O$	Ethanol + butyl carbitol (1:1 vol.) or ethanol + 1-methoxy-2-propanol	0.6 mm i.d.	7–30 kV (60 mm)	1.4–5.6 mL/h (60–120 min)		

(EDX), X-ray diffractometry (XRD), X-ray photoelectron spectroscopy (XPS), Fourier-transform infrared spectroscopy (FTIS), atomic force microscopy (AFM), transmission electron microscopy (TEM), or wavelength dispersion scanning (WDS).

Nuclear instruments

Initially, in 1950s and 1960s, the electrospray was used to produce thin films for nuclear-physics instruments. Carswell and Milsted [43] prepared layers for nuclear collision cross-section studies. The material to be deposited (U^{233}, Pu^{238}, Am^{241} or Cm^{242} nitrates) was dissolved in acetone and electrosprayed using a glass capillary with an ion injector made of a thin wire, which was connected to a high voltage dc source. The droplets evaporated without coalescence when they flowed to the substrate, and the material was deposited as a thin film. The layer was flat and of sharp edges.

This method was adopted for radioactive instruments production by Gorodinsky et al. [44]. The base of the spray plume was controlled by the variation of the distance between the capillary tip and the substrate. The differences in the layer thickness between the centre and the circumference of the deposit were lower than 20%. Bruninx and Rudstam [45] used electrospray to deposit thin uniform films for β counting. They tested over 40 substances dissolved in acetone, ethyl ether, ethyl acetate, ethanol, methanol or *n*-buthyl alcohol. The grain size was lower than 1 μm, and the samples were more even than those prepared by other methods. Michelson and Richardson [130] also prepared a β-source by this method. Lauer and Verdingh [46], and Reifarth et al. [81] produced neutron detectors using electrospray. The layer was perfectly stable, adherent to the substrate, and of homogeneity of the order of 1% [46].

Michelson [47], and Shorey and Michelson [48] produced neutron emitters from Uranium, Plutonium or Boron by using electrospray. Distilled water, formic acid, ethanol, methanol, isobutanol, *n*-butanol, ethylene dichloride, amyl alcohol, *n*-propanol, and isopropanol were tested as solvents. The film prepared by electrospraying consisted of fine (200 nm) uniformly sized, randomly oriented crystals of structure better than that obtained by vacuum evaporation method [130]. This technique was particularly attractive because the loss of the solute was small and the substrate was not overheated. Shorey and Michelson [48] noted that the spray system usually operated in the cone-jet mode for all the liquids tested. However, for liquids of dielectric constant lower than about 10, the multijet mode with two or three cones was observed.

A main advantage of preparation of thin radioactive sources by electrospraying is that the substance is not damaged, as it could be when chemical vapour or plasma spraying deposition would be used. The film thickness could be adjusted between 1 $\mu g/cm^2$ and 10 mg/cm^2 (cf. Table 1).

Solar cells

Since 1980s, the electrospray was tested as a new tool for preparation of thin films for solar cells. Mahoney and Perel [50], and Pang et al. [51] made the solar cells from silicone melted at a temperature of 1500°C, in a graphite vessel to avoid material contamination. The advantage of the electrospray was that the film was of lower porosity than that obtained by another method.

Since late 1990s the electrospray was used for production of solar cells from TiO_2 [42, 71], CdS [82, 84, 85], CdSe [83], or SnO_2 [90]. Films produced by electrospray were homogeneous and composed of agglomerates built of particles smaller than 1 μm, which were the dry powder particles used for preparing a suspension. The structure and optical properties of the CdSe films depend on the temperature and deposition method. For the electrospraying, the CdSe started to crystallise at the substrate temperature of 300°C and the number of crystals increased rapidly above 400 °C [82, 131]. For the films deposited at a temperature lower than 350 °C the CdSe grain size was below 100 nm, while for those deposited above 400 °C, was larger than 200 nm [83]. The CdS film deposited at a temperature of 250 °C was crystalline of hexagonal structure [84] but at 300 °C, the film was less crystallised with some pinholes on the surface. The film became smooth and well crystallised as the deposition temperature increased but at 450°C large particles could be formed on the smooth surface. The ZnS films deposited at 450°C contained crystallites with very small grain size of 20 nm, but at the substrate temperature of 500°C the grain size increased rapidly to about 80–200 nm [91].

The CdS and ZnS films were highly oriented in the electric field, but no preferred orientation was observed for the CdSe films. Due to the grain orientation of CdS and ZnS films in the electric field during precursors transformation to nanocrystals, they had good optical and opto-electrical properties for solar cell applications [85].

Fuel cells

Interest in production of electrodes and solid electrolytes for fuel cells by the electrospray deposition has

grown in recent years. The materials used for fuel cells fabrication were reviewed by Jiang and Chan [132]. Different thin-film deposition methods, such as CVD, PVD, RF sputtering, laser deposition, and casting, used for fuel cells production were presented by Will et al. [133]. However, the electrospray method has not been mentioned in these papers.

Electrostatic spray deposition was used to produce solid electrolyte for fuel cells from yttria-stabilised zirconia [35, 57, 65, 134], terbia-doped yttria-stabilised zirconia [60], barium cerate ($BaCeO_3$) [134], or gadolinia-doped ceria [34]. The details of the electrospray methods are cited in Table 1. The electrospray systems used for thin film deposition usually operated in a configuration with capillary facing upwards. The obtained films were amorphous or composed of nanocrystallites but could be annealed at higher temperatures to obtain the perovskite structure. For example, yttria-stabilised zirconia can be produced directly in the process of spraying, whereas barium cerate layer needs to be annealed [134]. Choy et al. [65] found that for the substrate temperatures lower than 500 °C, the electrospray-produced film of yttria-stabilised zirconia was amorphous or nanocrystalline, but after 2 h annealing at 800 °C the structure was changed to perovskite. However, at temperatures higher than 650 °C the perovskite could be obtained in one step that is an important advantage of the ESD. Nguyen and Djurado [100] observed that films of $ZrO_2 + Y_2O_3$ (yttria-doped-zirconia) were cracked with reticular outer layer when deposited at lower temperatures (300 °C). When the temperature was increased to 350 °C, cracks were formed in lower layer, and agglomerated particles have grown on its top. The cracks were attributed to the thermal stresses during the drying process. At 375 °C the cracks disappeared, and agglomerates were growing on the top of a dense layer. Taniguchi et al. [33, 34] concluded that the quality of the electrosprayed film for fuel cells was comparable or better than that obtained by laser-assisted deposition, magnetron sputtering, CVD, microwave plasma coating, or flame assisted vapour deposition.

Perednis et al. [35] compared the ESD with pressurised spray deposition technique. The morphology of the layers produced by ESD were dependent on the substrate temperature, precursor concentration and deposition time, whereas those prepared by the pressurised spray deposition not. The dependence of the ESD process on the substrate temperature was attributed to the solvent evaporation from the droplets approaching the substrate. Using an infrared pyrometer, the authors discovered that the gas temperature increased rapidly at the distance of 10 mm from the substrate, but for pressurised spray deposition this distance was only 5 mm due to the cooling effect of the nebulising gas. Additionally, the electrospray droplets were smaller than those produced by pressurised nebuliser that made evaporation faster. They also noticed that for higher precursor flow rates a porous film could be obtained when ESD technique is used. The film morphology in the pressurised spray deposition was less sensitive to the flow rate. The pressurised spray deposition could, therefore, be used for large area coating and for aqueous solution spraying but for precise coating of small areas the ESD is better.

Proton conducting membranes made of a polymer for fuel cells applications were fabricated by Sanders et al. [124]. The film was formed on a rotating PTFE-coated mandrel by coalescence of deposited droplets. The film thickness was approximately 50–60 μm. Nafion membranes produced by electrospray absorbed 15% by weight more water and exhibit diffusion coefficients higher by 30–70% compared to commercial membranes.

Lithium batteries

Van Zomeren et al. [28] were probably the first who used electrospray to produce electrodes for alkaline batteries. The spray system operated in the cone-jet mode, generating droplets of mean diameter of 4 μm. The film prepared by this method was of low porosity, with crystallites of average size of 0.3 μm. Interest in production of electrodes for lithium microbatteries by ESD deposition has grown in recent years. The demand for production of microbatteries is an effect of miniaturisation of electronic devices and a reduction of their power consumption.

Deposition of thin film of $LiMn_2O_4$ as a cathode for lithium ion batteries is usually accomplished by spraying a mixture of lithium acetate or nitrate, and manganese nitrate, as the precursors, which are dissolved in ethanol [70, 97–99, 109, 115–117]. For the production of $LiCoO_2$ cathodes, Chen et al. [29, 30, 55, 56], and Yoon et al. [102] used lithium acetate and cobalt nitrate dissolved in ethanol or ethanol and butyl carbitol mixture. The process took place at the ambient atmosphere and at a temperature in the range between 250 and 400°C. The film deposited by the ESD showed very stable charging/discharging characteristics. Dokko et al. [110, 111] produced $LiCo_xMn_{2-x}O_4$ cathodes from lithium, cobalt, and manganese nitrates dissolved in ethanol. Yamada et al. [80] tested $LiNiO_2$, $LiCo_{0.5}Ni_{0.5}O_2$, and $LiAl_{0.25}Ni_{0.75}O_2$ cathodes produced from lithium and nickel acetates, and cobalt and aluminium nitrates dissolved in ethanol. The cyclic voltammetry

and charge-discharge tests indicated that the films produced by ESD were electrochemically active for lithium ion extraction/insertion, similarly to conventionally fabricated cathodes. The substrate temperature for these processes is usually in the range of 250–500 °C.

Cao and Prakash [103] used the ESD to fabricate $LiMn_2O_4$ spinel thin films as a cathode for lithium batteries. The films showed similar electrochemical cycling profile as porous laminate films that could indicate structural similarity between them. The authors noticed that an organic binder and a carbon conductive additive, which could be found in a laminate film, were not present within the film prepared by ESD. These inclusions negatively affect the charging/discharging processes of a battery. Additionally, the size of the particles forming the layer was lower when the electrostatic deposition was used. The authors observed that the time constant of the diffusion processes is one order of magnitude larger for the film deposited by the electrostatic method than for the porous laminate film.

Two-layer structure comprising a cathode ($Li_xMn_2O_4$) and solid electrolyte (Li_xBPO_4) was prepared from lithium acetate and manganese acetate precursors by Chen et al. [61]. Kim et al. [113] tested vanadium pentoxide (V_2O_5) cathodes prepared by spraying of triisopropoxyvanadium oxide precursor dissolved in ethanol. The film exhibited a stable charge/discharge capacity during at least 25 cycles. Porous morphology of the film was beneficial for the lithium intercalation/de-intercalation from the positive electrode. The V_2O_5 film prepared by ESD method became crystalline at a temperature of 225 °C. This temperature was lower than that required by rf sputtering, pulsed laser deposition or electron beam evaporation processes, carried out at a temperature above 300 °C [113].

Anodes for rechargeable lithium-ion batteries made of SnO_2 were proposed and tested by Mohamedi et al. [96]. The film was prepared by the ESD at a temperature of 400 °C, followed by the layer annealing at 500 °C. The ESD deposited film was cycled electrochemically versus lithium and showed very good reversibility even at high current densities.

Micro- and nanoelectronic devices

In late 1990s, many authors have demonstrated the feasibility of atomising ceramic suspensions by electrostatic methods to produce thin isolation or semiconductor films, mainly for the purposes of electronic devices manufacturing. Metal oxide films, were made of, for example, TiO_2 [42, 64, 71, 91, 118, 135], ZrO_2 [31, 63, 72–75, 135], ZnO [31, 54], MgO [37, 38, 101], SnO_2 [67, 68, 86, 87, 90, 96, 121], CoO [31], $PbTiO_3$ [112], $BaZrO_3$ [136], or alumina [31, 104–108, 112, 119] (cf. Table 1). SiO_2 and ITO coatings of glass were made by Su and Choy [78], Chandrasekhar and Choy [88, 90], and Raj and Choy [89]. Semiconductor films made of CdSe [83, 131], SiC [72, 73, 75, 76, 137], CdS or ZnS [79, 82, 84, 91, 131, 138] were also prepared by electrospraying (cf. Table 1). Silicon and glass were most frequently used as the substrate in these experiments. The oxide layers were usually produced from fine metal-oxide powders, which after its deposition on a substrate were sintered to form a thin film.

TiO_2 is used for electronic devices manufacturing, for example, optoelectronic devices, solar cells, integrated circuits, as a dielectric in capacitors or field-effect transistors, gas sensors; and in materials engineering as a catalyst [42, 71, 91]. ZrO_2 films are applied as dielectrics in nanoelectronics due to a high dielectric constant of the material ($\varepsilon_r = 23$) and relatively high band gap, of about 5.8 eV. ZrO_2 is also used for fuel cells production [100], and for corrosion and thermal protection layers [74–76]. ZnO exhibits semiconducting, photoconductive, and piezoelectric properties, and, therefore, founded many applications in various fields of electronics, for transducers or sensors manufacturing [54]. MgO is used in plasma displays as a surface protection layer, as a buffer layer for high-temperature superconductors deposition, and as perovskite-type ferroelectric films [37, 38, 101]. $PbTiO_3$ [112] and $BaZrO_3$ [136] are deposited on a substrate as piezoelectric materials in sensors and microactuators.

Ryu and Kim [54] reported that the ZnO film deposited on silicon wafer at a temperature ranging from 230 to 450°C was composed of crystallites of mean size of about 20 nm, uniform, densely packed, pinhole-free, and predominantly c-axis oriented.

SnO_2 is used as an active layer in gas sensors, for example, for flammable and toxic gases [67, 68], CO_2 [93], and H_2 [67, 121]. It was also applied in electrochromic, photoluminescent phosphor, and liquid crystal displays, solar cells and heat mirrors [86, 87, 90]. However, Matsushima et al. [121] found that the sensitivity of a SnO_2 gas sensor produced by electrospray is lower than for those fabricated by an ion-beam sputtering method. This lower sensitivity was attributed to differences in the structure of primary particles formed in both processes, because the ESP process was carried out at relatively low temperature (500 °C). They also proved that the same effect took place when the crystallites were too large. The optimum size of the crystallites was found to be of about 10 nm. The ESP should, therefore, be optimised by decreasing the

precursor concentration, and improved by raising the substrate temperature. This requires using a quartz glass substrate, which is high-temperature resistant. It was noticed by Gourari et al. [67] that the sensitivity of SnO_2 gas sensor deposited on an alumina substrate to H_2 can be increased almost six times with an addition of manganese oxide, with the ratio of SnO_2:M-n_2O_3 = 10:1.

Recently, Kim et al. [120] using the ESD method, have produced an anhydrous and crystalline ruthenium oxide thin film electrodes with high specific capacitance ('supercapacitor'). The specific capacitance of anhydrous ruthenium oxide thin film was 500 F/g.

The electrospray was also used to fabricate more complex structures. Bi-layer ceramic films composed of ZrO_2 and SiC were produced by Miao et al. [75], and multilayer films of different materials were deposited on a substrate by Choy et al. [65], and Choy [139]. Such films can be easily deposited in consecutive processes by simple changing the precursor solution. The feasibility of production of mixed layers composed of crystallites of different materials, like, for example, SnO_2 + LaOCl [93] or ZrO_2 + Y_2O_3 [100, 139] by using the ESD was also demonstrated. The Y_2O_3:Eu films synthesised by Choy [91, 139] were amorphous when deposited at 400 °C, or of cubic form at 550 °C.

Fast development of polymer optoelectronic devices requires new, flexible and cheap technologies for their production. Denisyuk [58], and Cich et al. [66] tested the electrospray as a tool for the deposition of optically active layers on a flexible plastic material. The layer made by electrospraying was reproducible and the process was very efficient because at least 80% of the solution sprayed was deposited onto the substrate. The solution was sprayed from a dielectric nozzle in the axis of which an ion injector (a sharp needle) was placed. The thickness of the layer was between 1.5 and 5 μm with nonuniformity lower than 3% [58]. Cich et al. [66] produced a plasma display active layer deposited on Si(111) substrate. A precursor composed of zinc acetate, manganese acetate, and tetraethylorthosilicate dissolved in ethanol was electrosprayed from an upwards-facing glass capillary with a tungsten ion injector. After heating of the deposited film, an active layer of manganese doped zinc silicate $(ZnMg)SiO_4$ was obtained. The spraying process took place in an atmosphere of nitrogen and ethanol. The morphology of the layer and photoluminescence intensity were found to be dependent on the deposition conditions such as voltage and flow rate, and on the droplets' charge.

Heine et al. [69] used electrospray combined with CVD to incorporate photoluminescent CdSe quantum dots into ZnS matrix on a glass substrate. The quantum dots were encapsulated within a ZnS film of 100 nm thickness prepared by CVD method. The CdSe cores and ZnS coating were deposited simultaneously. Additionally, approximately 100 nm ZnS layer was grown using the electrospray technique, before and after the process of quantum dots forming, in order to encapsulate the CdSe dots in the ZnS matrix. By varying the size of the CdSe nanocrystals, the light could be tuned from blue to red. Films grown at 100 °C exhibited a hexagonal crystal structure (wurtzite) while those grown at higher temperatures have a cubic structure (zinc blend). At temperatures greater than 200 °C, films with a larger grain size were produced. Light intensity emitted by films grown at 250 °C was brighter than those deposited at 100 °C.

Biotechnology

In biotechnology, the electrospray was used, for example, to deposit biomolecules on a substrate for further studying them under a microscope or for medical diagnostics. For example, Thundat et al. [53] applied electrospray to the DNA molecules deposition onto a gold substrate for studies under a scanning tunnelling microscope. The electrospray, in comparison with standard electrodeposition or drop evaporation technique, offers more uniform sample distribution, isolated strands, and reduced number of molecular aggregates. A disadvantage of the method is that some of the strands can be distorted that masks intrinsic features of DNA.

The membranes for electroanalytical chemistry were prepared by Hoyer et al. [59]. The cellulose acetate phase inversion membranes on glassy carbon electrodes are used for electrodes protection in electroanalytical chemistry from fouling by macromolecular particles. Profilometric measurements showed that thin (300 nm) membranes were more uniform than those formed by solvent casting [59]. The ratio of the maximum to minimum thickness of the membrane ranged from 1.2 to 1.4, whereas for the membranes obtained by a conventional method the ratio of the thickness in the centre to that near the edge was up to five.

Moerman et al. [77, 94, 95] produced arrays of identical spots of 130–350 μm in diameter consisting of biologically active substances, such as enzymes or antibodies, for the purpose of their use in medical diagnosis, environmental research, or combinatorial chemistry. The substances remained biologically active after electrospraying, provided that the current is lower than 500 nA. The electrospraying in the stable cone-jet

mode allowed an accurate and reproducible dispersion of ultrasmall volume of liquid onto an array of spots without splashing, that is unobtainable by other deposition techniques, such as piezodispensing or contact-printing. The authors noticed that liquid droplets of a volume of 200 pL evaporate within 1 s at room temperature upon landing onto substrate. Thus, a dry reagent dot is obtained that preserves protein stability. The enzymes sprayed on-chip (silicon nitride) remained stable for a time of 1.5–2 months at a storage temperature of –20 °C [95].

Uematsu et al. [127] produced biologically active protein thin films for protein-based biomaterials, biosensors and biochips. The film was produced from α-lactalbumina. A fine porous (reticular) structure was obtained with pores in the size range of 40–600 nm. Tests indicated that the electrospraying had no effect on biological activity of the proteins.

The electrostatic spray deposition method was also used to produce ceramic calcium phosphate coatings on endosseous titanium implants [125, 126, 140]. No significant differences between the behaviours of the cells cultured on ESD and RF magnetron sputtered coatings were observed, although the two coatings differed in roughness, Ca/P ratio and molecular composition. The coatings were amorphous, irrespective of the initial Ca/P solution ratio, but they crystallised into different crystalline phases after annealing at 650 °C.

Other applications

Since 1990s the electrospray thin film deposition was used in many industrial applications such as materials technology and nanotechnology, for the production of solid lubricating films or photoresists. The electrospraying was also tested as a tool for electroprinting on solid surfaces.

Solid lubricating films of MoS_2 were obtained by electrospraying of MoS_2 dissolved in isopropanol, acetone, alcohol or toluene [39, 62]. In this process, the solvent evaporated when the droplets flowed to a grounded substrate, and only solid nanoparticles were deposited onto it. The film was composed of fine flat particles about 120 nm thick and with diameter up to 1000 nm. The film thickness was between 0.28 and 1 μm. The friction coefficient for stainless steel was in the range of 0.01–0.02 in a dry nitrogen atmosphere.

The production of thermal barrier coatings for protection of the components exposed to high temperature in gas turbines was demonstrated by Choy [139]. The layer consisted of yttria stabilised zirconia ($Y_2O_3 + ZrO_2$) doped with 1 mol.% of Eu. The coating was deposited on Ni based alloy substrate using the ESAVD. The author produced a single-layered and a double-layered coatings consisting of a thin Eu doped film and undoped film. The thermographic properties of the layer enabled measurement of the surface temperature up to 1100 K.

Recently, Lu et al. [104] produced piezoelectric microactuators made of zirconium *n*-propoxide, $Zr(C_3H_7O)_4$, titanium tetraisopropoxide, $Ti((CH_3)_2CHO)_4$, and lead acetate, $Pb(CH_3COO)_2$ for MEMS. The film deposited by electrospray had the crystallites of the size of about 150–200 nm. The film deposited at 100 °C consisted of particle agglomerates with spherical grains. At 25 °C, the film had dense microstructure and smoother surface morphology, and the grains were rhomboid with sharp boundaries. The difference in morphology was probably due to a longer time of interaction between the precursor droplet and the substrate that could take place at lower substrate temperatures. The permeation of the precursor solution through the earlier formed porous structure was deeper before the solvent evaporation.

Photosensitive resist (thin film deposited on a substrate and used as a mask, for example, in microelectronics or MEMSs) were prepared by electrospraying by Hall and Hemming [52]. The aerosol was sprayed by a centrifugal atomiser and charged by induction. Results showed that the layer was of sufficiently high quality, free of air entrapments, and its thickness was between 20 and 30 μm. Although this method was not purely electrohydrodynamic, it is expected that similar effects could be achieved with electrospray.

The cobaltite ($NiCo_2O_4$) electrocatalyst for oxygen reduction was fabricated by electrospraying from nickel and cobalt nitrates by Lapham et al. [32]. The size of the particles produced from the electrosprayed aerosol was smaller than the size of the particles generated by spray pyrolysis. As a result, the film has a larger contact surface area. Because the spraying process was accomplished at lower temperatures (350–400 °C) the spinel structure, required for electrocatalysis, was not damaged.

Jayasinghe et al. [119] studied the electrospraying of silica suspension in ethylene glycol, and Jayasinghe and Edirisinghe [128] alumina suspension in ethanol for the purpose of electrostatic printing on solid surfaces. The silica layer was deposited on a quartz glass, and alumina on a polymer substrate. The authors noticed that silica relics with diameter 1–80 μm were obtained from 0.5 to 20 μm droplets. The alumina relics were in the size range of 1–35 μm with mean diameter of 4–8 μm. Jayasinghe and Edirisinghe [106, 128] developed an electrostatic droplet concentrator consisting of a sharp needle placed behind the dielectric substrate, just in

the axis of the capillary nozzle. The grounded electrode helped to converge the spray in the target point on the substrate. However, the authors observed that finer droplets were difficult to converge and they were scattered around the target point. The flaw of the process was that silica relics were not homogeneous but contained an outer ring of the solvent (ethylene glycol) and small dense inner region of silica nanoparticles (20 nm in diameter).

Similar procedure of electrostatic printing of an organic material on ITO covered glass was developed by Saf et al. [123] for its application in molecular electronics. Oligo(methylmethacrilate) of degree of polymerisation $n = 9$ was dissolved in acetone and electrosprayed from a stainless steel capillary in N_2 gas at atmospheric pressure. The particles were dried on their way to the substrate, forming a film with a thickness between 30 and 130 nm, and roughness smaller than 1.3 nm. The novelty was that, using the electrostatic lenses, the spray was focused on the substrate surface, forming a spot of diameter 100 μm. Larger areas were covered by moving the substrate on an x–y table. Computer simulations indicated that the kinetic energy of the ions sprayed at atmospheric pressure is only a few electron-volts, which is sufficiently low to remain the substrate undamaged.

Fundamental studies

Electrospray experiments in thin film deposition can be categorised as either for the production of solid thin layers, or for fundamental studies of electrosprayed-film growth mechanisms, or a combination of both. The fundamental studies are aimed at better understanding of the layer formation processes, its morphology, and electrospray optimisation.

The layer formation is a complex and multi-step process, and, therefore, numerous explanations can be met in the literature. The morphology of the layer depends, in general, on the gas and substrate temperature, the solvent used for spraying, and the time of solvent evaporation from the layer. Chen et al. [141], and Schoonman [142] distinguished and drawn schematically four types of layer morphologies. But the research by Chen et al. [29–31, 55, 56, 61] and SEM photographs presented by, for example, Cich et al. [66], Gourari et al. [67], Diagne and Lumbreras [93], Yoon et al. [102], Miao et al. [75], Nguyen and Djurado [100], and Taniguchi et al. [33, 34], have indicated that other structures should be incorporated into this classification. The layer morphologies can be categorised into two main groups: dense and porous. The dense layer can be amorphous, crystalline (of different structures) or amorphous with incorporated particles (intrusions). The porous layer can be reticular, grainy, or fractal-like. These structures are schematically shown in Fig. 4. The morphology can change with the layer depth. Changing the physical properties of the liquid to be sprayed allows tailoring up to some extent the film morphology. Layer annealing at elevated temperatures, for 1 h or longer, can also modify the morphology, that was investigated by Chen et al. [30], and Yoon et al. [102].

The SEM images taken by Balachandran et al. [76] revealed that the ZrO_2 film was composed of agglomerates of the size of primary droplets, which in turn were built of powder particles, 0.5 μm in diameter, used for preparation of the suspension. The authors concluded that an advantage of spraying suspensions, instead of chemically prepared solutions, is the lack of chemical by-products, which could contaminate the film.

The substrate temperature is a critical parameter for film morphology. Nguyen and Djurado [100], and Huang et al. [112] observed that films prepared at too high temperatures consist of agglomerates, or are porous. On the other hand, Chen et al. [29], Kim et al. [37, 38], Zaouk et al. [86, 87], Rhee et al. [101] observed that films deposited at high temperatures become polycrystalline whereas those deposited at mediate substrate temperatures are amorphous. Chen et al. [30, 61], for example, noticed that at temperatures of 340 °C, in the case of $LiCoO_2$, the crystallites are formed. When the substrate temperature is extremely high (700 °C) only porous films can be obtained. The critical temperature depends on the material to be deposited. Chen et al. [31, 135] explained that when the ambient temperature is too high, the solvent evaporates too fast from the droplets, and only dry or

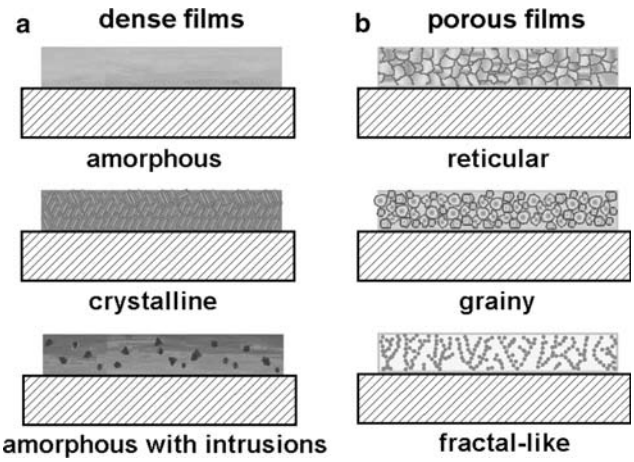

Fig. 4 Film structure morphologies: dense (**a**), porous (**b**)

semi-dry particles arrive at the substrate, forming a porous, fractal-like structure. Using a solvent of low evaporation rate (for example, a mixture of ethanol and butyl carbitol) makes evaporation slower, and the droplets can easily be spread on the surface, forming a dense amorphous film. Stelzer and Schoonman [60] reported that films with low porosity were produced when using a solvent with a high boiling point. They also noticed that the porosity of the substrate also could influence the film morphology. Raj and Choy [89] discovered that ITO surfaces consisted of crystalline and amorphous phases, and with an increase in the temperature (from 300 to 550 °C) the number of crystallites increased. At higher temperatures, the film was homogenous and had fairly uniform spherical grains of the size ranging from 250 to 850 nm.

Films of $PbTiO_3$ prepared by Huang et al. [107] at a temperature of 150 °C, which is slightly higher than the boiling point of the solvent (2-ethoxy ethanol), were smooth and dense but at higher temperatures (>150 °C) powder-like agglomerates composed of tiny particles were formed. Huang et al. [112] concluded that at high gas temperatures, the film became porous because mainly dry powder fell onto the substrate due to solvent evaporation from the droplets. Similar mechanism of porous film formation was also considered by Perednis et al. [35]. When solubility of a precursor is low, the precursor can precipitate within the droplet, and after impingement of such droplet onto the substrate, these fine crystallites could not be spread over the surface before ultimate drying.

The explanation of film formation mechanisms in the case of electrostatic-assisted CVD was proposed by Choy and Su [84]. At lower temperatures (300 °C for CdS) the charged aerosol is directly sprayed onto a substrate, followed by solvent evaporation and decomposition of the precursor. The film becomes porous and amorphous. At high substrate temperatures (450°C), the solvent vaporises and chemical precursors are decomposed before the droplet could impact on the heated surface. Then, only the solid particles are deposited on the substrate. The resultant film is porous, of powder-like structure. At intermediate temperatures both processes occur simultaneously, and small grains could be found at an amorphous film. The optimum temperature is, therefore, that at which the solvent evaporates close to the surface, and the decomposition and chemical reactions take only place at the substrate.

The layers can be distorted by cracks, voids or pinholes. The crack formation mechanism was proposed by Chen et al. [30]. At too low substrate temperatures, the solvent evaporation is slow and too much of it remains within the film, but after its evaporation the cracks are formed due to mechanical stresses. At higher temperatures the cracks disappear and the film becomes porous. Nguyen and Djurado [100], and Huang et al. [112] also noticed that too low temperatures cause the film cracking due to solvent accumulation on the surface. Huang et al. [112] proposed that the optimal deposition conditions are when the solvent evaporation rate is equal to the liquid deposition rate. Longer deposition times, with lower flow rates give, therefore, the layer more uniform, free of cracks and pores [33, 34]. Slow evaporation of the solvent helps to form a relatively dense film [103]. Choy et al. [65] noticed that multiple deposition, with subsequent sintering at an elevated temperature (1000 °C), for example, for 2 h, can also produce dense and crack-free films.

Recently, Perednis et al. [35] also investigated the effect of substrate temperature on film morphology. At too low temperatures (<200 °C) the solvent evaporated slowly and a thin wet layer remained at the surface. At too high temperatures (>350 °C) the droplets were almost dry when falling onto a substrate. Spreading of such droplets over the surface is difficult, and therefore, discrete, separated particles formed a porous or rough film. The authors found that an optimal temperature for dense film forming is in the range of 280 ± 50 °C. They also noticed that too fast drying of the film caused cracks. The results presented by Perednis et al. [35] are in opposite to those proposed by Chen et al. [141]. Chen and co-workers reported that solvent with a high boiling point has to be used in order to deposit a dense film. Perednis and co-workers concluded that the boiling point of the solvent has only its effect on the lowest possible deposition temperature required to obtain a dense, crack-free film. Their results indicated that the optimal temperature for the crack-free film deposition is slightly above the boiling point of the solvent.

Choy [91] observed that film morphology prepared by ESAVD depends not only on the substrate temperature but also on the precursor concentration. At low precursor concentrations (0.05 M of titanium diisopropoxide bis 2,4-pentanedionate in 2-proponol), the TiO_2 (anatase) films deposited at 400 °C were amorphous, but at higher concentrations, crystalline anatase films were formed. For the substrate temperature of 450 °C, an anatase film with crystallites of the size of about 10 nm was obtained. At higher precursor concentrations (0.2 M), the film was formed from crystal aggregates, with crystals of the size of 50–60 nm. The films composed of 10 nm particles were transparent and smooth whereas those build of crystal aggregates were opaque.

The problem of liquid evaporation during electrospraying was also considered theoretically and investigated experimentally by Grigoriev and Edirisinghe [143]. For the cone-jet mode, the liquid evaporation, heat lost in the needle and ambient air, and heat consumed by the emitted liquid causing an increase of its temperature were considered in the heat balance equations for the liquid meniscus. It was assumed that the Joule heating is the only heat source and that there lack of liquid bubbling. The problem of liquid evaporation is a vital one in the case of spraying of easily evaporating liquids, mainly hydrocarbons. For example, for toluene at the flow rate lower than 10^{-12} m^3/s, more than 10% of the liquid can evaporate from the meniscus. The authors also concluded that an increase in liquid conductivity results in higher thermal flux and rate of evaporation.

Chen et al. [135] have noticed that film morphology could be manipulated to some extent by adding some additives to the liquid. With the addition of acetic acid, routinely used for increasing liquid conductivity, to the ethanol solution, the structure of the layer was changed from severely cracked to crack-free reticular. This effect was attributed to the smaller droplets generation with acetic acid added. When ethanol is added to, for example, an aqueous solution, the solvent easier evaporates before the droplets are deposited on the substrate. Chandrasekhar and Choy [88] observed that a mixture of water and methanol used as a solvent for SnO_2:F thin film precursor, made the film rough and porous because of high surface tension of the solvent and its ability to dispersion into a large number of droplets in an electrospray system. A pure methanol was, therefore, recommended for a dense film production. Perednis et al. [35] noticed that an addition of 1% of polyethylene glycol to water solvent changed the yttria-stabilised zirconia film morphology from cracked to a crack-free. This was attributed to the binding properties of the polymer. The advantages and disadvantages of different precursors and solvents used for thin film deposition were discussed by Perednis et al. [35].

Morota et al. [122] have studied the effect of liquid physical properties such as viscosity, surface tension, conductivity, and molecular weight on nanostructured thin films morphology. The film was prepared by ESD from poly(ethylene oxide) in aqueous solution. By changing these properties and the applied voltage, the particles forming the layer can vary from nanospheres through nanospindles to nanofibers. The authors found that the use of alcohol as an additive to the polymer solution changed the viscosity, surface tension, and conductivity of the liquid, and helped to form the fibrous structure. An addition of hexanol reduced the surface tension of the solution without changing its viscosity and conductivity, but no effect of the surface tension on the film structure was observed. The effect of liquid viscosity was studied by changing the solution concentration within the range of 5 and 70 g/L that resulted in viscosity between 0.4 and 1410 mPa s. With an increase in polymer viscosity, the film structure changed from grainy composed of fine beads, to grainy composed of elongated spindles, and finally to a porous composed of fibres. For viscosity higher than 80 mPa s only polymer fibres were produced. The effect of solution viscosity on the film structure was also investigated by Perednis et al. [35]. With increasing viscosity, the spreading rate of the solution over the surface became lower, and, as a result, the film became rough. The conclusion was that the concentration of the precursor should not be too high when smooth, dense films are required.

The material to be sprayed can, at higher voltages, be damaged. Teer and Dole [49] studied the electrospray technique for the purpose of deposition of polystyrene latex particles on an aluminium foil. Electron microscope examination of the layer indicated that about 10% of the polystyrene beads was degraded at voltages higher than –24 kV. Spraying at positive voltage up to +20 kV, or in SF_6 atmosphere eliminated this degradation. The degradation was probably caused by bombardment of the droplets by electrons produced in the glow discharge in nitrogen, but the SF_6 gas quenched the discharge.

The film deposited by electrospraying can be contaminated due to solvent or precursor decomposition. Rutherford backscattering investigations of an MgO film, carried out by Rhee et al. [101], revealed that carbon impurities could be found in the film. These impurities were attributed to the precursor ($Mg(CH_3COO)_2$) decomposition. The content of carbon impurities decreased with an increase in the substrate temperature that allowed contaminants evaporation. Mohamedi et al. [96] observed some Cl impurities in a SnO_2 film when it was prepared from $SnCl_4$ precursor. X-ray photoelectron spectroscopy results obtained by Su and Choy [82] showed that a small amount of C, O and Cl impurities existed in the CdS film produced by ESAVD method as a result of the precursor decomposition. Additionally, the presence of C and O were attributed to the adsorption of CO_2 from the air. These impurities were removed by film sputtering with Ar atoms for 3 min.

It was proved by many authors that the quality of the thin film strongly depends on the size of the

particles or droplets forming the layer, their monodispersity, and their uniform distribution on the substrate. Smaller particles, having narrow size distribution, reduce the number and size of voids, flaws and cracks in the film. Uniform spatial dispersion of the droplets causes that the layer becomes more even and of the same thickness. All these properties affect the mechanical and electrical properties of the layer.

It can be concluded that electrospray allows production of extremely thin layers, which can be crack-free and more homogeneous than those obtained by other methods. The process is simple, cheap, flexible, and is easily controllable. Compared to other methods like CVD or PVD, its main advantage is that the growth rate of the layer is relatively high. The process can be carried out in an ambient atmosphere, in air or other gas, and at low temperature, without the need for a complex reactor and vacuum system. The deposited material is not damaged in this process that is important in the case of radioactive or biological substances. The ESD can produce highly pure materials with structural control at the nanometre scale. The crystallinity, texture, film thickness, and deposition rate can be controlled by adjusting voltage, flow rate, and the substrate temperature. Microscope inspections confirmed that the electrospray deposited layer is even, without micro-fissures and structural dislocations. The electrospray is a very efficient process because at least 80–90% of the solution can be deposited onto the substrate.

Many authors have optimised the electrospray process with regard to its application for thin film deposition. They made the observation that to obtain a dense, uniform film the deposition rate should be nearly equal to the solvent evaporation rate. For too low substrate temperature, cracks can be formed because the solvent remains on the substrate. For too high temperatures the droplets evaporate, and are deposited as solid particles forming a porous layer.

Although each research group reports the successful film deposition and fabricated device operation, most of them suggest that further development is required. Despite many experimental data, the definitive explanation of the electrospray mechanisms and film formation processes is not yet available.

Liquid metal ion and droplets sources

Introduction

Liquid Metal Ion Source (LMIS) is a device, which is used to produce a beam of metal ions, charged clusters, or charged nonodroplets from a molten metal. LMISs were introduced in 1970s, allowing development of focused ion beams (FIB) technology. LMISs have had significant impact on the semiconductor industry. Metal beams are used in micro- and nanoelectronics for the production of thin metal films, ion deposition and implantation, maskless doping, and direct writing. LMIS is also used for maskless etching of semiconductors, sputtering, scattering, micromachining, microlithography, patterning, and production of ultrafine metal powders [144]. LMISs are used in atomic physics, in secondary ions mass spectrometry, scanning ion beam microscopy [145, 146], and for surface coating [147].

Applications of LMISs in semiconductor industry, microelectronics and material technology were reviewed by Melngailis [148], Jeynes [149], Mair [150], Orloff [151], Stevie et al. [152], and Reyntjens and Puers [153]. Focused ion beam technology, including LMIS bibliography until 1990 was presented by Mackenzie and Smith [154]. Mitterauer [155] reviewed the designs and applications of microstructured multinozzle liquid metal ion and electron sources, and Gomer [156] the physical mechanisms of electron and ion generation from Taylor cones.

The metal ions are emitted from the tip of the Taylor cone with small jet-like protrusion at its apex formed at the outlet of a capillary nozzle, like in the electrospray devices, or from the apex of a solid needle covered with a liquid metal film. The difference between a LMIS and the electrospray of semiconducting liquids lies in that the meniscus and jet in the LMIS are primarily driven by Maxwell normal stresses whereas in the electrospray the tangential stress on the interphase surface is dominant. The voltage drop along the jet of the LMIS is lower than for other liquids, that is an effect of higher conductivity of metals [157, 158]. Three modes of droplet formation were, therefore, distinguished: detachment of the whole liquid cusp, detachment of droplets from the tip of the Taylor cone, and detachment of fine droplets from the shank of the Taylor cone and/or the needle or capillary emitter [cf. 158]. The third mode is only specific to the metal electrospray.

The volume flow rate is a parameter of minor importance in the LMISs than in other electrospray devices. The performances of a LMIS are characterised by the emission current, or the beam energy or its brightness. The brightness of LIMS is defined by the current I emitted by a source of an area A into a solid angle Ω [148]:

$$B = \frac{I}{A\Omega} \tag{6}$$

A typical LMIS consists of a nozzle made of tungsten or glass capillary of 0.02 to 0.2 mm i.d. through which the liquid metal flows, and an extractor electrode producing an electric field. A metal (usually tungsten) needle can be placed co-axially at the capillary outlet. A schematic diagram of the LMIS is shown in Fig. 5a. A schematic diagram of an ion emitter with a needle protruding from the capillary is presented in Fig. 5b. The emitted ions or droplets are accelerated by electric field of the extractor, and focused by electrostatic lens. Ions of different q/m can be separated by an E × B filter (cf. Fig. 5a), which combines electric and magnetic fields to select the ions of required magnitude of q/m. Only the ions of proper q/m can pass through the aperture in the mass separator, and other collide with the separator plate. Next, the ion beam can be deflected and focused onto the substrate.

Taylor cone is formed at the capillary outlet when the liquid metal is subjected to sufficiently high electric field. The Taylor cone is more stable for the nozzle with protruding needle than for a capillary with free meniscus. Van Es et al. [159] noticed that the liquid cone is the most stable when the cone angle of the needle is nearly equal to the angle of the Taylor cone, i.e., about 98°. In the needle ion emitter, a sharp regime of spraying conditions required for the stable Taylor cone formation is not necessary because the liquid is sprayed from the tip of the needle. A tungsten needle is usually used as such emitter because it is inert to most of metals and alloys. However, for the Sn emission, a nickel needle was recommended by Bischoff et al. [160].

Needles with rough surface have improved wetting properties and their operation is more stable than polished emitters. This effect was observed by Wagner and Hall [161], and Bell and Swanson [162]. Van Es et al. [159] have modified the emitter surface by making rough microchannels having length of several hundreds of micrometres and width of about 10 μm. These channels allowed supply of liquid metal along the needle cone to its apex by capillary action. This prevented off-axis ion emission and multiple Taylor cones forming, characteristic for the polished tips. The disadvantage of such microchannels is that they can be contaminated by the material of the extractor electrode sputtered due to ion bombardment. These contaminants can cause the blockade of flow of liquid metal.

Emitters with needle protruding from the nozzle were used as ion sources, for example, for scanning ion probe by Seliger et al. [163], for maskless ion implantation by Cheng and Steckl [164], for material surface studies by Prewett and Jefferies [165], and for micromachining, microlithography and metal implantation purposes by Benassayag et al. [166, 167]. In the early stage of LMIS development, the spot size was about 10 μm. The spot size of the Ga ion source used by Seliger et al. [163] and Prewett and Jefferies [165] was 100–500 nm, by the ion current density of about 1.5 A/cm^2. In recent years there is a growing interest in nanotechnology in designing LMISs producing ion beam of the spot size smaller than 10 nm [153, 159, 168, 169].

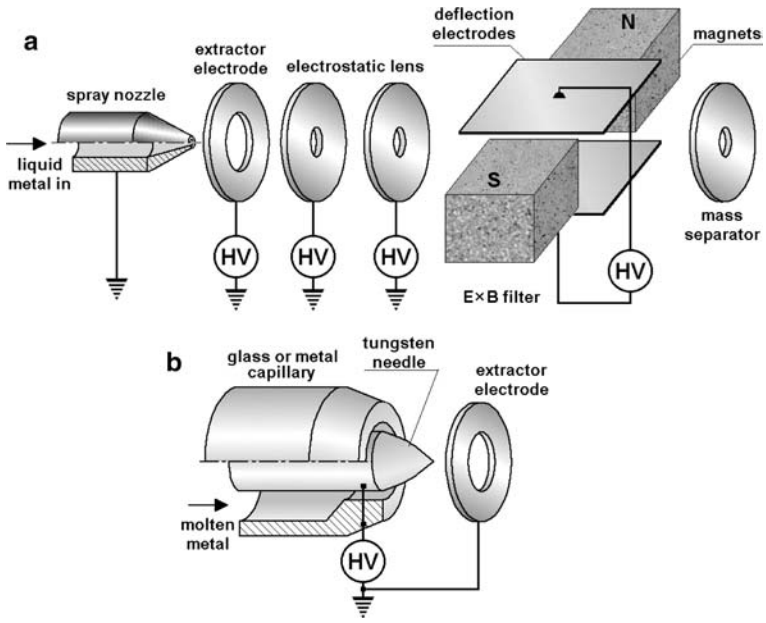

Fig. 5 Liquid metal ion sources: capillary nozzle—ions are focused and separated with electrostatic lenses and E × B filter (**a**), capillary nozzle with a needle emitter (**b**)

Many modifications to the devices based on the principle of spraying from a needle tip were proposed in the literature. Vladimirov et al. [170] used a steel needle of tip radius of 10 μm protruding from a graphite container. The liquid metal was evaporated due to additional sputtering by electron bombardment. Longitudinal groves on the needle surface were etched in order to decrease the flow resistance of the metal. Purcell et al. [171] covered a tungsten W(111) needle of 50 nm tip radius with the metal to be sprayed (Au or Ag). The metal was deposited on the emitter by evaporation from a circular loop surrounding the emitter tip. The emission took place due to field desorption of metal atoms from the cone apex. This source could operate at least 10 h with a stable emission current in the range of 1–3.5 pA. This ion source was designed for ion implantation or nanowiring in nanotechnology.

In order to avoid generating large droplets, which can be produced while spraying from a capillary facing downwards, Clampitt and Jefferies [172] developed a liquid metal ion source with a needle placed in a vessel and protruding above a molten metal surface (Fig. 6). The ions were extracted from the needle tip wetted with the molten metal, by the electric field produced by the extractor electrode. The tip of the needle should be sufficiently sharp in order to a single cusp to be formed at the needle tip. The device has an advantage of not requiring a capillary for liquid metal supplying, but the shortcoming is that this ion source can operate only in one position. Liquid Cs, Ga and Hg were tested as ion sources. This type of metal ion source is characterised by high purity, low power consumption, and long lifetime.

Hairpin emitter was designed by Wagner and Hall [161] for emission small amounts of liquid metal in vacuum conditions. This type of emitter is made in the form of tungsten hairpin with a tungsten sharp needle at its tip (Fig. 7). The molten metal is held at the hairpin free-end due to the surface tension force. To increase the volume of such reservoir a small coil was mounted beneath the needle or the end of the wire is twisted to a double-coil [160]. The liquid metal flows to the needle tip due to capillary forces, and ions are extracted by an electric field. The hairpin is usually resistively heated to melt the metal in the reservoir but can also be melted due to electron bombardment [173, 174].

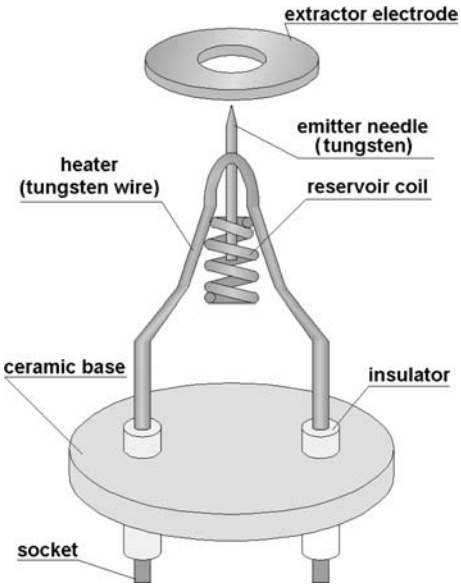

Fig. 7 Hairpin-type liquid metal ion source

To obtain high emission currents for metal film deposition on large areas, a multiple emitter can be used [175]. However, Mitterauer [155] applied a porous material as ion emitter (Fig. 8). The nozzle was

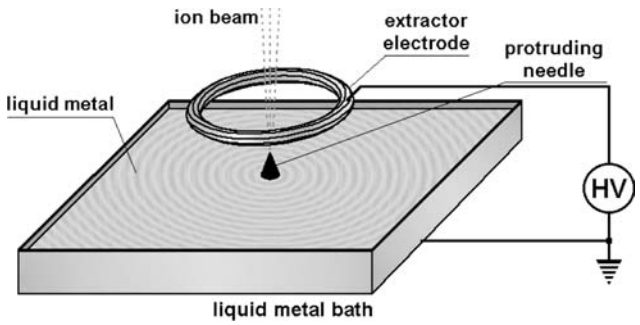

Fig. 6 Liquid metal ion source; molten metal sprayed from a cone-needle [cf. 172]

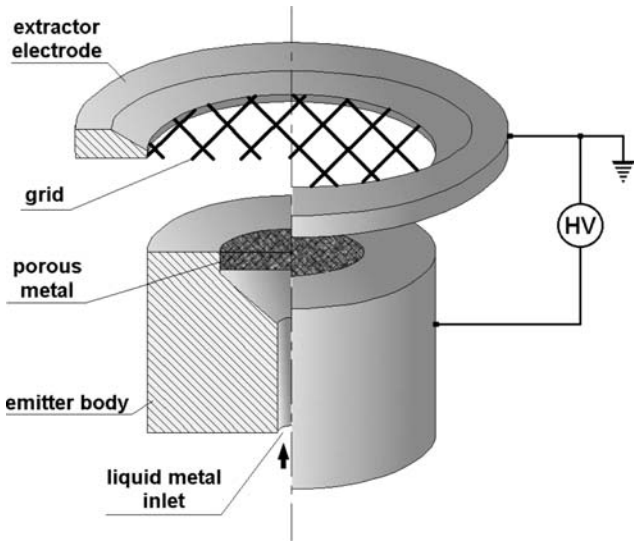

Fig. 8 Liquid metal ion source with porous metal emitter [cf. 155]

made of sintered Iconel 600 with the grain size between 10 and 50 μm. Each grain at the surface of such material can be a potential emission site. The number of such sites was estimated to $4 \times 10^4/cm^2$. The mean emission current from this emitter was 20 nA/site. The extractor electrode was made of stainless steel plate with a grid made of stainless steel wire. The grid width was 2 mm, and the distance between the grid and the porous emitter was 2 mm. Earlier, similar sintered porous material for an ion emitter was proposed and tested by Ishikawa and Takagi [176]. The emitter was made from sintered tungsten powder of the grain size in the range of 10–100 μm. The flow rate of the liquid metal to the tip was dependent on the diameter of the powder.

LMISs are usually excited with DC voltage but an AC excitation was tested by Bahasadri et al. [177]. They applied AC voltage of frequency of 4 kHz, which affected the size of the droplets, whereas dc bias voltage allowed controlling the liquid flow rate.

The emission current is typically in the range from a few picoamps to milliamps, but the current density can be as high as 5 kA/cm^2. The LMIS brightness is typically of about 10^6–10^7 $A/cm^2/sr$. The details of liquid metal ion sources, which are discussed in this paper, are summarised in Table 2.

Thin metal film deposition

In this section, an overview of the application of liquid metal ion sources to thin film deposition is briefly presented. Metal thin films are, for example, used as microelectrodes in electrochemistry, resistors and wires in microelectronic devices, optical reflection layers in optoelectronic devices, and layers of specific adsorption and adhesion properties [144]. LMISs are used for direct film deposition or, more frequently, as ion emitters for FIB technology.

Mahony and Prewett [181] applied a liquid metal source for deposition of Au conducting paths in hybrid microelectronic circuits. Better adhesion to the substrate was obtained by this method compared to a conventional one. The authors used an emitter needle of tip radius of 70 μm. For the emission current lower than 200 μA only metal ions were emitted. Above 600 μA, a stable, simultaneous emission of microdroplets and ions was observed.

Niobium LMIS for FIB deposition of superconducting thin film was developed by Nagamachi et al. [183, 184]. The beam diameter of Au^+, Cu^+, Al^+, and Nb^{2+} ions was between 0.5 and 8 μm. The Nb^{2+} ion beam was extracted from the $Nb_{10}Au_{50}Cu_{40}$ alloy with E × B filter. A Wehnelt electrode maintained at +1.1 kV was used to eliminate secondary electrons. The extractor electrode was at the potential of –6 kV relative to the ion source.

Arnold and Balachandran [147] constructed an electrohydrodynamic atomiser made of molybdenum for direct deposition of gold microporous membranes. The membranes were produced by electrospraying of gold droplets onto a stainless steel fibre mat. The deposition process took about 1 h. The size of the particles deposited was smaller than 1 μm.

Hu et al. [198] compared the properties of Au layers deposited on pyrolitic graphite using two techniques: a LMIS and pulsed laser ablation. A tantalum hairpin emitter was used as the LMIS. The tip of the needle was heated by the electron bombardment. The LMIS-produced Au clusters (Au+, Au_3^+, Au_7^+) were of the size of 3.5–6.5 nm (5.3 nm median diameter). The size distribution of the clusters emitted by the LMIS was narrower than for the clusters prepared by laser ablation, although the laser (KrP excimer laser, 248 nm, 10 ns pulse) could produce smaller clusters. The thickness of the Au film was of about 2 atomic layers. Au^+ ions and Au_3^+ and Au_7^+ clusters were also produced by Saito et al. [188]. The ions were deposited on a highly-oriented-pyrolytic graphite and amorphous carbon. The energy of the ions was up to 500 eV, but for the clusters only 5 eV. For the ion energy higher than 100 eV, the graphite surface was damaged. Depending on the ion energy, the size of the clusters deposited on the amorphous carbon was 0.5–20 nm, and on the graphite 2–5 nm. The authors noticed that with the time elapsed, the deposited clusters have a tendency to coagulate, forming, after 10 months, larger spherical clusters of diameter of about 20 nm.

The Coulomb-blockade devices were produced by Vieu et al. [187]. The authors used a hairpin ion emitter for depositing Au nanodroplets on a substrate. They noticed that for low emission currents (< 40 μA), when the energy of the particles impinging on the substrate was sufficiently low to avoid their fragmentation, the film could be deposited in the form of isolated grains of the size of about 1 nm.

A method of film deposition on large surface area (60 cm^2) was developed by Yamaguti [173]. The metal to be sprayed was placed in a carbon crucible, and heated by electron bombardment. The molten metal formed a droplet of about 6 mm in diameter. The extractor electrode was in the form of straight wires 0.5 mm in diameter, placed 10 mm above the crucible. The device produced droplets smaller than 1 μm. For all the metals tested (cf. Table 2), the ion source current was between 0.3 and 12 mA, and the growth rate

Table 2 Liquid metal ion sources

Authors	Metal	Nozzle	Voltage	Ion beam current (current density)	Ion energy (Brightness)	Spot/beam size (cluster size)
Mahoney et al. [178]	Cs, Rb, K, Na, Tl, Li, Ga, Pb, Bi, Cd, Sn, Hg	Tungsten capillary 0.04 mm i.d. 0.11 mm o.d.	7.5 kV	140 μA (10^4 A/cm^2)		(not focused)
Evans and Hendricks [179]	GaIn	Stainless steel capillary (#28) 0.178 mm i.d. 0.356 mm o.d.	13 kV (extractor plate, 6 mm aperture)	30 μA	(2.6×10^6 A/cm^2/sr)	
Colby and Evans [145]	GaInSb BPbSnCdIn		8–13 kV	75 μA		
Krohn and Ringo [146]	Ga, Cs, Hg	Tungsten capillary 0.1 mm o.d.	–21 kV (extractor plate, 0.12 mm aperture)	1–200 μA (C_s,H_g)10–200 μA (Ga)	12 eV (Ga) 15 eV (Cs) (0.9×10^5 A/cm^2/sr)	15 μm
Yamaguti [173]	Pb, Ag, Pt, Sb, Zn, Au, Al., Fe, Ni, Sn, W, C (2×10^{-3} Torr)	Carbon bath (electron bombardment heating)	1 kV (10 mm to extractor made of a pair of tungsten wires 0.5 mm dia.)	1–10 mA		(0.1–0.5 μm grains)
Clampitt and Jefferies [172]	Cs, Ga, Hg, In	Needle protruding above liquid metal surface	2–10 kV	20 μA	0.1–25 keV	
Seliger et al. [163]	Ga	Capillary reservoir, tungsten needle	5–7 kV	10 μA (1.5 A/cm^2)	(3.3×10^6 A/cm^2/sr)	100–500 nm (@ 0.12–3 nA)
Prewett and Jefferies [165]	Ga, Au	Capillary reservoir, tungsten needle 0.3 mm (5–10 μm tip radius)	4–10 kV (molybdenum extractor disk, 1.5 mm aperture)	10–100 μA 10–50 μA/sr (Ga) 5–35 μA/sr (Au)	100 eV–10 keV	500 nm (@ 0.5 nA)
Mair and von Engel [180]	Ga	Capillary reservoir, tantalum needle 0.3 mm dia. (20 μm tip radius)	6–9 kV (extractor plate, 2 mm aperture)	2–200 μA (0.4×10^{-10} kg/s)		
Mahony and Prewett [181]	Au	Needle emitter (70 μm tip radius)	13 kV	<200 μA (ions) >600 μA (ions + droplets)		300 μm
Benassayag et al. [166,167]	Ga, Au	Hairpin emitter, tungsten needle 50 μm	4.6–6.2 kV (Ga) 15–20 kV (Au)	1–300 μA (2.16–3.6 nl/h)	(10^8 A/cm^2/sr) – Ga (6.7×10^5 μm^3/s/sr) – Ga 600–1000 μm^3/s – Au (1.5 μm^3/s –deposition rate)	5 μm (Au) (0.25–2 μm Au droplets) (0.27–6 μm film thickness)
D'Cruz et al. [182]	Au	Needle tip		100–250 μA	(5×10^3 μm^3/s deposition rate)	(0.1–1.5 μm clusters)
Vladimirov et al. [170]	Sn (5×10^{-6} Torr)	Graphite container, protruding steel needle (10 μm tip radius)	6–8 kV (extractor, 2.5 mm aperture)	40–100 μA (2.5–4.6×10^4 C/kg)		(1–30 nm droplets)
Nagamachi et al. [183,184]	Au, Cu, Al, Nb, $Nb_{10}Au_{50}Cu_{40}$		–6 kV	40 pA–10 nA	20 keV	500–8000 nm beam diameter
Arnold and Balachandran [147]	Au	Molybdenum nozzle, 0.1 mm i.d. 0.15 mm o.d.	10–20 kV (1.5 mm to extractor of 3 mm aperture)	500 μA (0.48–2.3×10^4 C/kg)		(0.8 μm droplets)

Table 2 continued

Authors	Metal	Nozzle	Voltage	Ion beam current (current density)	Ion energy (Brightness)	Spot/beam size (cluster size)
Mitterauer [155]	Cs	Porous emitter disk (10–50 μm grain size) (5 mm dia., 2 mm thick.)	10 kV (emitter) 2 kV (extractor) (2 mm emitter-extractor)	30 μA (20 nA/site)		
Chen et al. [185]	Sn(57%)Pb alloy (400 °C)	Orifice nozzle 0.1 mm dia.	(66.7 or 94.4 kV/m) (270 or 480 mm to substrate)		(179 μm/s deposition rate)	20 mm (198 μm droplets)
Driesel et al. [186]	Pb, Ga, In, Sn, AuSi, AuGe, CoGe, CoNd	Hairpin emitter tungsten needle	4.19–5.2 kV (1.5 mm)	3–60 μA		
Vieu et al. [187]	Au (10^{-8} Torr)	Hairpin emitter	1–15 kV (10 V/nm)	20–100 μA	0.5–10 keV	(1–4 nm grains)
Saito et al. [188]	Au (10^{-7} Torr)				500 eV (ions) 5 eV (clusters) (90 s – Au^+, 45 min – Au_3^+, 3.5 h – Au_7^+ deposition time)	0.5–20 nm (clusters on amorphous carbon), 2–5 nm (clusters on graphite)
Sazio et al. [189]; Vijendran et al. [190]	AuSiBe	Hairpin emitter		8 μA	(1 μm/h growth rate)	160 nm Be^{2+} doped layer, 100 nm Si^{2+} doped layer
Gierak et al. [169]	Ga	Hairpin emitter	9–17.5 kV	2 μA (20–90 μA/sr)	30 keV	10 nm
Cheng and Steckl [164]	Ga_2Mg (GaN doping with Mg) (10^{-7} Torr)	Hairpin emitter, tungsten needle (10 μm tip radius)	+1.1 kV (3.5 mm to Wehnelt electrode with 3 mm aperture) –6 kV to –12 kV (28.5 mm to extractor electrode with 1.85 mm aperture)	30 μA	30–100 keV	
Reyntjens and Puers [153]	Ga	Tungsten needle wetted by molten metal	7 kV	2 μA	10–50 keV	<10 nm (@ 1 pA–10 nA)
Purcell et al. [171]	Au, Ag (7×10^{-7} Torr)	Tungsten wire (50 nm tip radius)	1.3 kV (Au) 1.1 kV (Ag)	1–3.5 pA	11–12.6 eV (5×10^5 A/cm^2/sr)	5.4–53 nm (with lenses) 5–25 nm (near-field)
Akhmadaliev et al. [191–193]; Mair et al. [194,195]	Ga, AuGe, Au(77%) Ge(14%) Si(9%) (7×10^{-7} Torr)	Hairpin emitter, tungsten wire, 0.2 mm dia. (5–10 μm tip radius)	8–10 kV (0.5 mm to extractor with 1 mm aperture or 50 mm to the collector)	1–100 μA		
Bischoff et al. [160]	Sn	Hairpin emitter, nickel wire 0.3 mm dia.	5.3–6.3 kV	2–50 μA		
Bischoff et al. [196]	$Au_{82}Si_{18}$ (850°C)		4.78 kV	30 μA		
Van Es et al. [159]	Ga (10^{-6}–10^{-10} Torr, 300 K)	Hairpin emitter, tungsten needle 0.1 mm (0.1–2 μm tip radius) 49° half angle	–5–17 kV (to extractor)	2–60 μA	25 keV (20–80 μA/sr)	10 nm
Vijendran et al. [197]	GaMn (450–500 °C)	Hairpin emitter, tungsten wire	–6 kV (to extractor)	>10 μA		5 μm

between 0.8 nm/min (for W) and 1.75 μm/min (Sb). Most metals were deposited as nearly spherical particles of the size smaller than 1 μm, but Sb, Zn, and Sn were in the form of elongated spindles of the length 1–2 μm, and the axis ratio between 3 (Sb) and 7 (Zn). It was supposed by the author that these particles solidified during their flight to the substrate. Yamaguti [173] also observed that for extremely high emission currents, > 10 mA, and at low temperatures, metals of high vapour pressure are ejected from the liquid phase as large droplets, and form a thick film on the substrate. Materials of low boiling point are deposited as particles of large mass. Their mass increases exponentially with the metal density decreasing.

The LMISs are also used for ion implantation in semiconductor devices. Ion implantation is a technique of adding ions to a lattice of semiconductor crystal in order to modify its electronic properties. Nowadays, ion implantation is the most attractive maskless doping method because it offers an advantage of direct placing of any ion at various depths in a semiconductor lattice, independently of thermodynamic problems of diffusion. Although the ion beam can partly damage the Si structure, most of these defects can be repaired by annealing at a temperature of 700–1000 °C [144].

The LMIS applications for ion implantation have a numerous literature, and will not be discussed here. The only exception is the selective ion doping during epitaxial growth of a semiconductor, a method developed by Sazio et al. [189] and Vijendran et al. [190]. It is a single step process, which does not require a photolithographic mask. An $Au_{70}Si_{15}Be_{15}$ LMIS was used for *n* (Si) and *p* (Be) selective doping in a single (100)GaAs epilayer after E × B mass filtration. It is difficult to produce such layers by conventional lithographic techniques. The most abundant Be^{2+} and Si^{2+} dopants with landing energy of 30 and 25 eV, respectively, were used. The technique minimises structure damage in comparison to thermally doped materials or post-growth dopant ion implantation, which require energies of about 100 keV. Using the same method, the authors were able to construct a 3D buried microstructures with complex topologies, or heterostructures doping for optoelectronic applications. This technique was adopted by Vijendran et al. [199] for the production of an optical modulator with electrically controlled optical absorption coefficient. The structure consisted of 40 alternate *p-i* and *n-i* layers. Vijendran et al. [197] used also a hairpin emitter made of tungsten wire covered with Ga (90% by weight) and Mn (10%) alloy as a source of Mn dopant for production magnetic elements in a GaAs lattice during its epitaxial growth.

Fundamental studies

The current-voltage characteristics, effect of emitter temperature and electrode geometry on emission current, and the effect of the emission current on source stability have been the most important operating properties of LMISs studied in order to understand the ion emission processes and optimise the emitter devices.

Properties of charged metal droplets produced by an electric discharge in vacuum were first investigated by Krohn [200]. The droplets of Wood metal were in the size range of 5 to 15 nm. He noticed that capillary emitter produced as well charged droplets as metal ions, and their proportion was depended on the extractor voltage. The current-voltage characteristics of a capillary type LMIS were determined by Mair [201]:

$$I = 3\pi\left(\frac{2e}{m}\right)^{1/2}\frac{\left(\frac{U}{U_0}-1\right)}{U_0^{1/2}}R\sigma_l\cos\varphi \tag{7}$$

where σ_l is the liquid metal surface tension, m is its molecular mass, R is the base radius of the Taylor cone, ϕ is the half-angle of the Taylor cone, and U_0 is the spray onset voltage.

The LMISs operate only in a limited range of emission current. Krohn and Ringo [146] observed that below 1 μA for Cs and 10 μA for Ga, the Taylor cone collapsed and the ion source ceased emitting. The turn-on current for GaMn alloy measured by Vijendran et al. [197] was 10 μA. It its now commonly accepted and evidenced experimentally that a certain minimum emission current exists, for most metals usually higher than 1–2 μA, at which operation of the LMIS is stable [159, 160, 202–205]. At lower currents, the source operates in the pulsating mode because the liquid metal surface oscillates due to hydrodynamic instabilities, and droplet emission from the base of the Taylor cone can be observed [159, 170, 206]. Vladimirov et al. also observed that the crest of the capillary could be an additional source of droplets. The current oscillations were in the kHz range [205].

In fact, the emission current is a function of the electric field at the Taylor cone surface, and this quantity or the extractor potential should be used as a parameter when considering LMIS stability, but the emission current is traditionally commonly used.

On the other extreme, for currents higher than 50–100 μA, the pulsating emission was also observed. Such instabilities were noticed for Ga and Cs ion sources by Krohn and Ringo [146] for the currents above 200 μA. For these currents, the source started to emit droplets. Mair and von Engel [180] observed fluctuations up to about 20% for currents higher than 100 μA. The fluctuations were attributed to electrohydrodynamic instabilities of the jet, which started to break up into droplets. Bahasadri et al. [177] noticed that for the currents higher than a few tens of μA, a significant portion of mass from the LMIS was emitted in the form of atom clusters or fine droplets. It was attributed to cavitations of liquid metal due to high electrostatic pressure that exists on the Taylor cone.

D'Cruz et al. [182] supposed that emission of clusters and droplets is mainly confined to the tip of the cone. However, Gabovich [207] (cf. also Gabovich and Poritsky [208]) examined the surface of a LMIS under a SEM, and showed that for the emission current density 100 A/cm^2, droplets and clusters can be ejected simultaneously from numerous sites on the surface of the cone. The emission sites were smaller than 1 μm in diameter.

Driesel et al. [186] observed liquid Pb, Ga, In, Sn, AuSi, AuGe, CoGe, CoNd emitters under a TEM. The authors noticed that the Taylor cone shape was dependent on the voltage, and the metal to be sprayed. The authors suppose that the differences in the shape are caused by the space charge, which reduces the electric field on the cone tip. Heavier ions are more inert, and it takes a longer time to remove them to the counter electrode. The ions form, therefore, a more stable space charge. For Pb, for example, the half-angle decreased from 50,5 to 46.2°, when the emission current increased from 3 to 39 μA. For currents higher than about 28 μA, the droplets emission from the cone sides was also observed. The size of the droplets was in the range of 40–340 nm. Praprotnik et al. [209] have shown the photographs on which the In droplet emission can be observed for the current as low as 2.8 μA. Driesel and Dietzsch [210], for Sn emitter, observed droplets emission for the current of 4 μA. The authors also shown that for intermediate emission currents (> 38 μA), double cone can be formed. Purcell et al. [171] observed that single emission point at the cone tip could be obtained only in a limited range of voltage. For too low voltages, two off-axis emission points were photographed. For higher voltages, the emission current was saturated, and three emission points were formed.

Nowadays it is assumed that at high-current regime, the cluster generation is caused by high electrostatic pressure that exists on the Taylor cone. This pressure pulls out small fragments of liquid metal. This unstable emission of droplets causes that the emission current is pulsed. Vladimirov et al. [170] recorded oscillations of the electric field near the ion emitter in two frequency bands: 1–10 GHz, and 1–10 MHz. The high-frequency oscillations were attributed to detachment of the droplets from the cone apex and their fission. Low-frequency oscillations were caused by periodic oscillations of the jet length. The variations of the jet length were caused by the space charge of the emitted droplets, which reduced the electric field near the Taylor cone. Also from TEM micrographs taken by Bischoff et al. [211] resulted that the LMIS jet became longer and thicker with the excitation voltage and emission current increasing. This was due to an increase in the electric field at the emitter tip. However, at a certain voltage, the field decreased and the tip of the jet became blunt.

Mair [212] and Hesse et al. [213] observed the current pulses, but in different frequency ranges. For the emission current of 50–200 μA, the high frequency band was in the range of 1 to 5 MHz, and the low frequency in the range of kHz. They observed that the ionic current pulses were negative at the Ga beam centre and positive at the beam edges. The negative pulses were due to the shielding effect of the departing droplets. Similar results were presented by Mair [206], Mair et al. [195], and Akhmadaliev et al. [191, 192]. The pulses in the 1 MHz frequency range were attributed to the droplet emission, which coincided with the frequency of the Taylor cone vibration. The high frequency mode, about 10 MHz, was explained by the process of disintegration of the original charged droplet into smaller ones. The peaks at 30 MHz were tentatively explained as caused by the jet vibration.

The equation of critical current for oscillations was given by Mair [206]:

$$I_c = 13.4\pi \frac{e}{m} \frac{\rho_l^{1/2} \sigma_l^2}{\varepsilon_0^{3/2} E_i^3} \tag{8}$$

where m is the ion mass, ρ_l and σ_l are the liquid density and surface tension, respectively, r_j is the emitter jet radius, and E_i is the evaporation field, which assumes the values of the order of magnitude of 10^{10} V/m. From this equation Mair concluded that the metals with high surface tension, low evaporation field and small ionic mass are more stable against the electrohydrodynamic instabilities.

Degree of ionisation of the metal ions was first investigated by Mahoney et al. [178]; and Evans and

Hendricks [179]. Metals of the I group (Cs, Rb, K, Na, Tl, Li, Ga) can emit only atomic ions, sometimes multiply charged (for example, Cs^{2+} and Cs^{3+}, Ga^{3+}, Ga^{2+}, In^{3+} and In^{2+}), while those of the II group (Pb, Bi, Cd, Sn, Hg) can produce charged particles of the size ranging from atomic ions to multi-atomic clusters and charged droplets. Prewett and Jefferies [165] noticed that a Ga ion source can produce mainly single charged ions whereas Au emitter generates multiply charged ions and charged molecular clusters. The degree of ionisation depends also on the emission current. Bischoff et al. [211] measured the Sn^{2+}/Sn^{+} ratio as a function of the emission current. Initially this ratio increased, and for the emission current of about 6 μA started to decrease.

At present, it is well known that not only singly or doubly charged ions, metal clusters or fine droplets are emitted by LMISs but also neutral atoms or their clusters. Mair and von Engel [180, 214] discovered that at low emission currents, up to about 100 μA, for each emitted ion, one or two neutral atoms were released, some of them in excited states. The number of neutrals increased for higher currents, and, for example, for 200 μA, there was about ten times more neutrals than ions. Similarly, Thompson [215] showed that the number of neutral atoms emitted for each ion is always greater than unity. This ratio also increased with emission current, from about 1 at low currents, to 8 at a current of 70 μA. Mair and von Engel [180], Barr [216], and Bahasadri et al. [177] noticed that for the emission current higher than a few μA, a significant portion of mass is emitted in the form of clusters or fine droplets.

Forbes [158] suggested that neutrals emission is mainly in the form of microdroplets, which are detached from the Taylor cone or from the shank of the emitter. This phenomenon cannot be observed for the electrospray of semi-insulating liquids because the droplets are emitted only from the end of the jet.

Ion formation in LMIS is another key issue associated with the use of LMISs. Forbes [158], in his review paper, distinguished two mechanisms of ionisation. The first one is the field evaporation, which is a single-stage process in which breaking of the atom–surface bonds and ionisation of the atom take place simultaneously. The second mechanism is the surface field ionisation, which is a two-stage process. In the first stage a neutral atom is detached from the surface (due, for example, to its thermal energy), and in the second stage it is ionised, probably due to tunnelling of an electron from the atom to the emitter. The surface field ionisation takes place at lower fields than the field evaporation. After an ion detachment, an ionisation to double and higher states can take place. This process is called ''post-ionisation''. It is supposed that post ionisation is an effect of electron tunnelling from the ion back to the emitter. The tunnelling can take place at distances of a few atom radii from the surface [217, 218].

Swanson and Kingham [219], and Kingham and Swanson [220, 221] considered theoretically the problem of ion formation and concluded that field evaporation is the main ion formation mechanism. The second most important is the field ionisation of thermally evaporated neutrals. However, Aidinis et al. [204] investigating the emission of Ge^{+} and Ge^{2+} ions, and Bischoff et al. [160, 211] measuring mass spectra of Sn^{+} and Sn^{2+} have concluded that both ions are produced as a result of direct field evaporation from the liquid surface, rather than post-ionisation of a singly ionised atom. Aidinis et al. [204] noticed that for a current of about 6 μA the doubly charged ions dominated by the factor of two. Bischoff et al. [211] detected also the singly charged Sn clusters, up to Sn_7^{+} in the ion beam. The charged cluster formation was interpreted as a result of fine droplets disintegration by an ion impact. Mair et al. [218] proved theoretically and experimentally both processes and concluded that they are equally possible, but for different species. For example, the Ge^{2+} and Si^{2+} ions are produced due to direct field evaporation whereas Au^{2+} is formed by the post-ionisation of Au^{+} ion (cf. also Ganetsos et al. [222]). For a eutectic alloy of $Au_{82}Si_{18}$, Bischoff et al. [196] obtained Si^{2+} ions due to field evaporation, and Au^{2+} ions produced by post ionisation of Au^{+}.

Mair et al. [194, 195], and Akhmadaliev et al. [191, 193] studied the effect of an extractor electrode on the spraying process in a LMIS of Ga, AuGe, and AuGeSi alloys. When the extractor electrode was removed, the amplitude of the current pulses was larger, and the pulses were of shorter duration. Because of ion scattering by the space charge generated by the droplets, not only negative but also positive amplitudes of the pulses were observed. The shorter duration of the pulses was probably caused by less effective shielding of the cone tip by the droplets. This could imply that individual droplets are smaller and therefore can be removed quickly from the vicinity of the emitter. The authors also observed that with increasing current the jet became thicker and the droplets larger. The larger droplets were removed slowly from the vicinity of the cone and the frequency spectra shifted to lower values.

The effect of ion source temperature on emission current was investigated by Bischoff et al. [196, 223], Mair et al. [194], Akhmadaliev et al. [192], and Aidinis [224, 225]. With a temperature increasing the jet and cone become unstable, presumably because the surface tension of the molten metal is reduced [192]. The value

of critical current also decreases [192, 193, 213]. Beckman et al. [202] noticed that the transition current and current pulse amplitude increase with the source temperature, and that for a given metal, the emission current is independent of the apex radius or the emitter surface roughness.

In summary, it can be concluded that the advantage of electrospray as a source of liquid metal ions is a small amount of metal sample necessary for ion production. Higher adherence to the substrate was obtained by this method as compared to conventional ones. The brightness of a LMIS is usually higher than plasma sources, sometimes almost two orders of magnitude, with similar energy consumption [146]. Typical voltage applied between the nozzle and extractor electrode is 5–10 kV, and the emitter-extractor distance is usually from 1 to 5 mm that gives the electric field at the apex about 10^9–10^{10} V/m. The apex and jet radii are in the range of 0.1 to 1 μm. The liquid metal film on a needle-type ion emitter is thinner than 1 μm. FIB technology based on LMIS is capable to produce ion beam as fine as 10 nm. Besides many publications devoted to the conditions of ions and clusters generation the problem is still not sufficiently recognised.

Electrospray forming

Since late 1980s, fine droplets were used for spray forming, although first experiments with thermal spray to produce solid bodies were carried out in 1924 by Turner and Ballard [cf. 226]. In the spray forming, a molten metal is atomised into spray of droplets, which are deposited onto a substrate to form a condensed product. Spray forming is a means for direct layer-by-layer production of bulk materials or thick coatings at an industrial scale. During this process, the solid powders, semi-solid and fully liquid droplets impacting a surface mix in the way, which is similar to the liquid phase sintering [227].

Metal sheets, pipes, rolls or huge billets can be formed from steel alloys, cooper alloys or aluminium alloys [228]. The products can be manufactured directly from the molten metals. Spray forming offers a possibility of production of alloys of controlled microstructure and composition down to molecular layers. The method is particularly suitable for the production of difficult-to-form materials. By simultaneous spraying of metal droplets and powder components, for example ceramics, which are difficult to mix by other ways, a composite material can directly be deposited. Spray forming was used for composite materials production from alumina–titania [226] or aluminium-rutile [229]. Nowadays, billets with diameters up to 500 mm and weight of 4 t are produced [230]. However, the process can also be used for production of miniature multilayer circuits, functionally graded materials, composites or small complex-shaped elements when only the destination of each droplet could be controlled [63].

Spray forming is not a perfect process because a porous deposit could be formed. Voids and pores restrict the technology mainly to volume products. The defects are caused by various droplets sizes and their thermodynamic states. Production of thin films or sheets requires special precautions and post-forming processes, for example, annealing at elevated temperatures. If the spray is produced by pneumatic atomisation, the gaseous entrapments of the size as large as 40–80 μm can also be found in the microstructure [229]. The overall solid fraction at the point of deposition is usually between 40 and 90% [231]. Centrifugal atomisation in vacuum was one of the remedies [232] but its application is limited to large surfaces. In conventional spray forming systems, up to 40–50% of the powder is oversprayed, and re-injection of the powder was proposed by Schneider et al. [233] to increase the overall efficiency of the process up to 85%.

The comparison of spray forming technology with conventional casting was performed by Yu et al. [227], Srivastava et al. [234], Chaudhury et al. [229], and Mesquita and Barbosa [230]. From these considerations it was concluded that the spray formed materials have higher isotropy, can be of lower porosity, and their microstructure is more uniform. The process of cooling is faster without material strength. The hardness of the spray formed composite can be greater, and the particles in the matrix are distributed more uniformly. The composition of such materials can be changed on demand during the production process.

Using electrospray for spray forming was proposed by Chen et al. [185]. The advantage of the electrospray is that the droplets are uniform in size, and have similar thermodynamic states that would reduce the number and size of voids in the bulk material. The apparatus used by Chen and co-workers produced droplets by agitation of a jet with a piezoelectric transducer tuned to 10 kHz, and charged them by induction. For mushy droplets, the SnPb alloy deposit structure was equiaxed with crystals of random orientation. The equiaxed microstructure is formed when droplets solidify and crystallise before they impact onto a surface. When the metal was fully molten, the structure was epitaxial columnar. The deposit was non-porous. The process took place in $N_2 + 2\%H_2$ atmosphere. Considering various experimental conditions, Chen et al. [185]

concluded that a coarse solidification structures are produced when hot droplets are deposited onto a hot substrate, while porous structure, when cold droplets fall on a cold substrate. An optimal situation, an equiaxed-grains structure, can be found between these two extremes.

Recently, Jayasinghe and Edirisinghe [106, 235] used electrospray for forming porous ceramic materials. Alumina slurry of mean particle size of 0.5 μm containing 21% by volume of solids was used for ceramic foam production. The electrosprayed droplets were deposited onto a polyurethane substrate used as a pre-former. The substrate was next heated for an hour to 900 °C for soaking, and to 1400 °C for host material pyrolyses. The porosity was about 96%. The specimen was build of struts 100 μm thick, and it was homogeneous and crack free. The process was easy to replicate. This technique was adopted by Jayasinghe and Edirisinghe [108] for forming microsized channels. The droplets of alumina suspension of mean particle size of 7 μm were deposited on a pre-former, an organic fibre, which was next pyrolysed at a temperature of 1400 °C. The material was sprayed for 1 h, and dried 1/2 h. The spraying/drying process was repeated 3 times for multilayer channel production.

Although electrospray is hitherto not widely used for spray forming, it is believed that all liquid metal ion sources can be applied for spray forming, particularly for a microscale production. This process could be called 'electrospray forming'.

Conclusions

Electrospraying was proved to be a versatile tool for various material processing technologies. A number of established and emerging electrospray applications for thin film deposition have been presented. The goal of this review was to provide a summary of electrospray applications in thin solid film deposition. A large number of examples of practical significance, or only laboratory-scale experiments have been given. The presented methods are compared in Tables 1 and 2. Electrospray has advantages of uniform coating of large areas, inexpensive equipment, operation at atmospheric conditions, and easy control of deposition rate and film thickness by adjusting voltage and flow rate. Advances in electrospray applications in thin film deposition will certainly continue in near future, particularly in nanotechnology and biotechnology, and new achievements in this field can be expected.

However, there are still a number of challenges to be faced, needed for commercial thin film production. One of such problems is a specific electrospray mode control. Electrospray is very sensitive to the liquid physical properties and the electric field in the vicinity of the emitter tip. The issue of continuous control of spray modes has been undertaken by Valaskovic et al. [236]. An orthogonal opto-electronic system based on the spray plume observation in certain characteristic cross sections, which controls the applied voltage has been developed. For further development in MEMS, nanotechnology, and nanoelectronics it will be necessary to develop the direct patterning techniques for the deposition of thin layers of pattern size finer than 1 μm.

Although an attempt was made to consider wide spectrum of relevant refereed papers, the literature cited in this paper is by no means complete. However, the author believes that it should provide the reader with the development and application of electrospraying, including LMISs, in thin film deposition.

References

1. Rayleigh FRS (1882) Phil Mag 14(5):184
2. Lapple CE (1970) In: Drew TB, Cokelet GR, Hoopes JW Jr, Vermeulen T (eds), Advances in chemical engineering, vol 8. Academic Press, New York, London
3. Jaworek A, Adamiak K, Krupa A, Castle P (2001) J Electrostatics 51–52:603
4. Bailey AG, Bracher JG, von Rohden HJ (1972) J Spacecraft 9(7):518
5. Snarski SR, Dunn PF (1991) Exp Fluids 11(4):268
6. Rulison AJ, Flagan RC (1993) Rev Sci Instrum 64(3):683
7. Franks A, Luty M, Robbie CJ, Stedman M (1998) Nanotechnoly 9(2):61
8. Almekinders JC, Jones C (1999) J Aerosol Sci 30(7):969
9. Regele JD, Papac MJ, Rickard MJA, Dunn-Rankin D (2002) J Aerosol Sci 32(11):1471
10. Krupa A, Jaworek A, Czech T, Lackowski M, Luckner J (2003) Inst Phys Conf Ser 178:283
11. Jaworek A, Balachandran W, Lackowski M, Kulon J, Krupa A (2006) J Electrostatics 64(3–4): 194
12. Sato M (1991) IEEE Trans Ind Appl 27(2):316
13. Balachandran W, Krupa A, Machowski W, Jaworek A (2001a) J Electrostatics 51–52:193
14. Balachandran W, Jaworek A, Krupa A, Kulon J, Lackowski M (2003) J Electrostatics 58(3–4):209
15. Law SE, Cooper SC (1988) Trans ASAE 31(4):984
16. Law SE, Cooper SC, Law WB (1999) Inst Phys Conf Ser No 163:243
17. Law SE (2001) J Electrostatics 51–52:25
18. Hayati I, Bailey AI, Tadros ThF (1987) J Coll Interface Sci 117(1):205
19. Cloupeau M, Prunet-Foch B (1990) J Electrostatics 25:165
20. Cloupeau M, Prunet-Foch B (1994) J Aerosol Sci 25(6):1121
21. Grace JM, Marijnissen JCM (1994) J Aerosol Sci 25(6):1005
22. Jaworek A, Krupa A (1996a) J Aerosol Sci 27(1):75
23. Jaworek A, Krupa A (1996b) J Aerosol Sci 27(7):979
24. Jaworek A, Krupa A (1999a) Exp Fluids 27(1):43
25. Jaworek A, Krupa A (1999b) J Aerosol Sci 30(7):873

26. Altenburg H, Plewa J, Plesch G, Shpotyuk O (2002) Pure Appl Chem 74(11):2083
27. Choy KL (2003) Progress Mater Sci 48:57
28. Zomeren van AA, Kelder EM, Marijnissen JCM, Schoonman J (1994) J Aerosol Sci 25(6):1229
29. Chen CH, Buysman AAJ, Kelder EM, Schoonman J (1995) Solid State Ionics 80:1
30. Chen CH, Kelder EM, Jak MJG, Schoonman J (1996b) Solid State Ionics 86:1301
31. Chen CH, Emond MHJ, Kelder EM, Meester B, Schoonman J (1999a) J Aerosol Sci 30(7):959
32. Lapham DP, Colbeck I, Schoonman J, Kamlag Y (2001) Thin Solid Films 391:17
33. Taniguchi I, van Landschoot RC, Schoonman J (2003a) Solid State Ionics 156:1
34. Taniguchi I, van Landschoot RC, Schoonman J (2003b) Solid State Ionics 160:271
35. Perednis D, Wilhelm O, Pratsinis SE, Gauckler LJ (2005) Thin Solid Films 474:84
36. Park H, Kim K, Kim S (2004) J Aerosol Sci 35(11):1295
37. Kim SG, Choi KH, Eun JH, Kim HJ, Hwang ChS (2000a) This Solid Films 377:694
38. Kim SG, Kim JY, Kim HJ (2000b) This Solid Films 378:110
39. Sorensen G (1999) Surf Coat Techn 112(1–3):221
40. Li JL (2005) J Aerosol Sci 36:373
41. Kessick R, Fenn J, Tepper G (2004) Polymer 45:2981
42. Choy KL, Su B (1999) J Mater Sci Lett 18:943
43. Carswell DJ, Milsted J (1957) J Nucl Energy 4:51
44. Gorodinsky WA, Romanov JuF, Sorokina AW, Yakunin MI (1959) Prib Techn Exper 5:128
45. Bruninx E, Rudstam G (1961) Nucl Instrum Methods 13:131
46. Lauer KF, Verdingh V (1963) Nucl Instrum Methods 21:161
47. Michelson D (1968) J Fluid Mech 33(3):573
48. Shorey JD, Michelson D (1970) Nucl Instrum Meth 82:295
49. Teer D, Dole M (1975) J Polymer Sci 13(5):985
50. Mahoney JF, Perel J (1981) IEEE Ind. Appl. Soc. Conf. Rec., 1142–1145
51. Pang TM, Prewett PD, Gowland L (1982) This Solid Films 88:219
52. Hall A, Hemming M (1992) Circuit World 18(2):32
53. Thundat T, Warmack RJ, Allison DP, Ferrell TL (1992) Ultramicroscopy 42–44(Pt. B):1083
54. Ryu ChK, Kim K (1995) Appl Phys Lett 67(22):3337
55. Chen CH, Kelder EM, Schoonman J (1996c) J Mater Sci 31(20):5437
56. Chen CH, Kelder EM, Schoonman J (1997a) J Mater Sci Lett 16:1967
57. Chen CH, Nord-Varhaug K, Schoonman J (1996e) J Mater Synth Process 4(3):189
58. Denisyuk IYu (1996) J Opt Technol 63(4):296
59. Hoyer B, Sorensen G, Jensen N, Nielsen DB, Larsen B (1996) Anal Chem 68(21):3840
60. Stelzer NHJ, Schoonman J (1996) J Mater Synth Proc 4(6):429
61. Chen CH, Kelder EM, Schoonman J (1997b) J Power Sources 68:377
62. Sobota J, Sorensen G (1997) Tribology Lett 3:161
63. Teng WD, Huneiti ZA, Machowski W, Evans JRG, Edirisinghe MJ, Balachandran W (1997) J Mater Sci Lett 16:1017
64. Chen CH, Yuan FL, Schoonman J (1998b) Eur J Solid State Inorg Chem 35:198
65. Choy K, Bai W, Charojrochkul S, Steele BCH (1998) J Power Sources 71:361
66. Cich M, Kim K, Choi H, Hwang ST (1998) Appl Phys Lett 73(15):2116
67. Gourari H, Lumbreras M, Van Landschoot R, Schoonman J (1998) Sensors Actuators B 47:189
68. Gourari H, Lumbreras M, Van Landschoot R, Schoonman J (1999) Sensors Actuators B 58:365
69. Heine JR, Rodriguez-Viejo J, Bawendi MG, Jensen KF (1998) J Crystal Growth 195(1–4):564
70. Nishizawa M, Uchiyama T, Dokko K, Yamada K, Matsue T, Uchida I (1998) Bull Chem Soc Japan 71(8):2011
71. Chen CH, Kelder EM, Schoonman J (1999b) Thin Solid Films 342:35
72. Miao P, Huneiti ZA, Machowski W, Balachandran W, Xiao P, Evans JRG (1999) Inst Phys Conf Ser No 163:119
73. Miao P, Balachandran W, Xiao P (2002) IEEE Trans Ind Appl 38(1):50
74. Miao P, Balachandran W, Wang JL (2001a) J Electrostatics 51–52:43
75. Miao P, Balachandran W, Xiao P (2001b) J Mater Sci 36:2925
76. Balachandran W, Miao P, Xiao P (2001b) J Electrostatics 50(4):249
77. Moerman R, Frank J, Marijnissen JCM, van Dedem GH (1999) J Aerosol Sci 30(Suppl. 1):551
78. Su B, Choy KL (1999a) J Mater Sci Lett 18:1705
79. Turetsky AYe (1999) J Aerosol Sci 30(Suppl. 1):689
80. Yamada K, Sato N, Fujino T, Lee ChG, Uchida I, Selman JR (1999) J Solid State Electrochem 3:148
81. Reifarth R, Schwarz K, Käppeler F (2000) Astrophys J 528(1):573
82. Su B, Choy KL (2000a) Thin Solid Films 359:160
83. Su B, Choy KL (2000b) J Mater Sci Lett 19:1859
84. Choy KL, Su B (2001) Thin Solid Films 388:9
85. Su B, Wei M, Choy KL (2001) Mater Lett 43:83
86. Zaouk D, Zaatar Y, Khoury A, Llinares C, Charles JP, Bechara J (2000a) Microelectr Eng 51–52:627
87. Zaouk D, Zaatar Y, Khoury A, Llinares C, Charles JP, Bechara J (2000b) J Appl Phys 87:7539
88. Chandrasekhar R, Choy KL (2001a) Thin Solid Films 398–399:59
89. Raj ES, Choy KL (2003) Mater Chem Phys 82:489
90. Chandrasekhar R, Choy KL (2001b) J Crystal Growth 231:215
91. Choy KL (2001) Mater Sci Eng C 16:139
92. Wei M, Choy KL (2002) Chem Vapor Depos 8(1):15
93. Diagne EHA, Lumbreras M (2001) Sensors Actuators B 78:98
94. Moerman R, Frank J, Marijnissen JCM, Schalkhammer TGM, van Dedem GWK (2001) Anal Chem 73(10):2183
95. Moerman R, Knoll J, Apetrei C, van den Doel LR, van Dedem GWK (2005) Anal Chem 77:225
96. Mohamedi M, Lee SJ, Takahashi D, Nishizawa M, Itoh T, Uchida I (2001a) Electrochimica Acta 46:1161
97. Mohamedi M, Takahashi D, Uchiyama T, Itoh T, Nishizawa M, Uchida I (2001b) J Power Sources 93:93
98. Mohamedi M, Takahashi D, Itoh T, Uchida I (2002a) Electrochimica Acta 47:3483
99. Mohamedi M, Takahashi D, Itoh T, Umeda M, Uchida I (2002b) J Electrochem Soc 149(1):A19
100. Nguyen T, Djurado E (2001) Solid State Ionics 138:191
101. Rhee SH, Yang Y, Choi HS, Myoung JM, Kim K (2001) Thin Solid Films 396(1–2):23
102. Yoon WS, Ban SH, Lee KK, Kim KB, Kim MG, Lee JM (2001) J Power Sources 97–98:282
103. Cao F, Prakash J (2002) Electrochimica Acta 47:1607

104. Jayasinghe SN, Edirisinghe MJ, DeWilde T (2002) Mat Res Innovat 6(3):92
105. Jayasinghe SN, Edirisinghe MJ, Kippax PG (2004a) Appl Phys A 78:343
106. Jayasinghe SN, Edirisinghe MJ (2002) J Porous Mater 9:265
107. Jayasinghe SN, Edirisinghe MJ (2003) Mat Res Innovat 7:62
108. Jayasinghe SN, Edirisinghe MJ (2004) J Europ Ceramic Soc 24:2203
109. Kobayashi Y, Miyashiro H, Takeuchi T, Shigemura H, Balakrishnan N, Tabuchi M, Kageyama H, Iwahori T (2002) Solid State Ionics 152–153:137
110. Dokko K, Anzue N, Makino Y, Mohamedi M, Itoh T, Umeda M, Uchida I (2003) Electrochem 71(12):1061
111. Dokko K, Anzue N, Mohamedi M, Itoh T, Uchida I (2004) Electrochem Comm 6:384
112. Huang H, Yao X, Wu X, Wang M, Zhang L (2003) Microelectr Eng 66:688
113. Kim YT, Gopukumar S, Kim KB, Cho BW (2003) J Power Sources 117:110
114. Lu J, Chu J, Huang W, Ping Z (2003) Sensors Actuators A 108:2
115. Shu D, Chung KY, Cho WI, Kim KB (2003a) J Power Sources 114:253
116. Shu D, Kumar G, Kim KB, Ryu KS, Chan SH (2003b) Solid State Ionics 160:227
117. Chung KY, Shu D, Kim KB (2004) Electrochim Acta 49:887
118. Hou X, Choy K-L (2004) Surface Coat Technol 180–181:15
119. Jayasinghe SN, Edirisinghe MJ, Wang DZ (2004b) Nanotechnology 15:1519
120. Kim IH, Kim KB (2004) J Electrochem Soc 151(1):E7
121. Matsushima Y, Nemoto Y, Yamazaki T, Maeda K, Suzuki T (2004) Sensors Actuators B 96:133
122. Morota K, Matsumoto H, Mizukoshi T, Konosu Y, Minagawa M, Tanioka A, Yamagata Y, Inoue K (2004) J Colloid Interface Sci 279:484
123. Saf R, Goriup M, Steindl T, Hamedinger TE, Sandholzer D, Hayn G (2004) NatMat 3(5):323
124. Sanders EH, McGrady KA, Wnek GE, Edmondson CA, Mueller JM, Fontanella JJ, Suarez S, Greenbaum SG (2004) J Power Sources 129:55
125. Siebers MC, Walboomers XF, Leeuwenburgh SCG, Wolke JGC, Jansen JA (2004) Biomater 25:2019
126. Leeuwenburgh SCG, Wolke JGC, Schoonman J, Jansen JA (2004) Biomater 25:641
127. Uematsu I, Matsumoto H, Morota K, Minagawa M, Tanioka A, Yamagata Y, Inoue K (2004) J Colloid Interface Sci 269:336
128. Jayasinghe SN, Edirisinghe MJ (2005a) Appl Phys A 80:399
129. Dorey RA, Whatmore RW (2004) J Electroceramics 12:19
130. Michelson D, Richardson OW (1963) Nucl Instrum Methods 21:355
131. Su B, Choy KL (2000c) Thin Solid Films 361–362:102
132. Jiang SP, Chan SH (2004) J Mater Sci 39(14):4405
133. Will J, Mitterdorfer A, Kleinlogel C, Perednis D, Gauckler LJ (2000) Solid State Ionics 131:79
134. Kelder EM, Nijs OCJ, Schoonman J (1994) Solid State Ionics 68(1–2):5
135. Chen CH, Kelder EM, Schoonman J (1998a) J Europ Ceramic Soc 18:1439
136. Su B, Choy KL (1999b) J Mater Chem 9(7):1629
137. Grigoriev DA, Edirisinghe M, Bao X (2002) J Mater Res 17(2):487
138. Su B, Choy KL (2000d) J Mater Chem 10(4):949
139. Choy KL (2000) Surf Eng, 16(6):469
140. Leeuwenburgh S, Wolke J, Schoonman J, Jansen J (2003) J Biomed Mater Res A 66A(2):330
141. Chen CH, Kelder EM, vanderPut PJJM, Schoonman J (1996d) J Mater Chem 6(5):765
142. Schoonman J (2000) Solid State Ionics 135:5
143. Grigoriev DA, Edirisinghe M (2002) J Appl Phys 91(1):437
144. Madou MJ (2002) Fundamentals of microfabrication. CRC Press
145. Colby BN, Evans CA Jr (1973) Anal Chem 45(11):884
146. Krohn VE, Ringo GR (1975) Appl Phys Lett 27(9):479
147. Arnold PG, Balachandran W (1995) Electrostatics Inst. Phys. Conf. Ser. No. 143:283–288
148. Melngailis J (1987) J Vac Sci Technol B5(2):469
149. Jeynes C (1989) Vacuum 39(11–12):1047
150. Mair GLR (1992) Int J Mass Spectr Ion Proc 114(1–2):1
151. Orloff J (1993) Rev Sci Instrum 64(5):1105
152. Stevie FA, Shane TC, Kahora PM, Hull R, Bahnck D, Kannan VC, David E (1995) Surf Interface Anal 23(2):61
153. Reyntjens S, Puers R (2001) J Micromech Microeng 11(4):287
154. Mackenzie RAD, Smith GDW (1990) Nanotechnology 1(2):163
155. Mitterauer J (1995) Appl Surf Sci 87–88:79
156. Gomer R (1979) Appl Phys 19(4):365
157. Forbes RG (1997) Vacuum 48(1):85
158. Forbes RG (2000) J Aerosol Sci 31(1):97
159. Van Es JJ, Gierak J, Forbes RG, Suvorov VG, Van den Berghe T, Dubuisson Ph, Monnet I, Septier A (2004) Microelectr Eng 73–74:132
160. Bischoff L, Akhmadaliev C, Mair AWR, Mair GLR, Ganetsos T, Aidinis CJ (2004a) Appl Phys A 79:89
161. Wagner A, Hall TM (1979) J Vac Sci Technol 16(6):1871
162. Bell AE, Swanson LW (1986) Appl Phys A 41:335
163. Seliger RL, Ward JW, Wang V, Kubena RL (1979) Appl Phys Lett 34(5):310
164. Cheng J, Steckl AJ (2001) J Vacuum Sci Technol B19(6):2551
165. Prewett PD, Jefferies DK (1980) J Phys D: Appl Phys 13(9):1747
166. Benassayag G, Sudraud P, Jouffrey B (1985) Ultramicroscopy 16(1):1
167. Benassayag G, Orloff J, Swanson LW (1986) J Physique C7 47(Suppl. 11):389
168. Davies ST, Khamsehpour B (1996) Vacuum 47(5):455
169. Gierak J, Septier A, Vieu C (1999) Methods Phys Res A427:91
170. Vladimirov VV, Badan VE, Goshkov VN, Soloshenko IA (1993) Appl Surf Sci 65/66(1–4):1
171. Purcell ST, Binh VT, Thevenard P (2001) Nanotechnology 12(2):168
172. Clampitt R, Jefferies DK (1978) Nucl Instrum Methods 149:739
173. Yamaguti T (1977) Japan J Appl Phys 16(9):1547
174. Noda T, Okutani T, Yagi K, Tamura H, Okano H, Watanabe H (1982) Rev Sci Instrum 53(9):1482
175. Ishikawa J, Tsuji H, Aoyama Y, Takagi T (1990) Rev Sci Instrum 61(1, pt.2):592
176. Ishikawa J, Takagi T (1984) J Appl Phys 56(11):3050
177. Bahasadri A, Brown WL, Saedi R, Pourrezaei K (1988) J Vac Sci Technol B6(6):2085
178. Mahoney JF, Yahiku AY, Daley HL, Moore RD, Perel J (1969) J Appl Phys 40(13):5101
179. Evans CA Jr, Hendricks CD (1972) Rev Sci Instrum 43(10):1527

180. Mair GLR, von Engel A (1981) J Phys D: Appl Phys 14(9):1721
181. Mahony C, Prewett PD (1984) Vacuum 34(1–2):301
182. D'Cruz C, Pourrezaei K, Wagner A (1985) J Appl Phys 58(7):2724
183. Nagamachi S, Yamakage Y, Ueda M, Maruno H, Shinada K, Fujiyama Y, Asari M, Ishikawa J (1994) Appl Phys Lett 65(25):3278
184. Nagamachi S, Yamakage Y, Ueda M, Maruno H, Ishikawa J (1996) Rev Sci Instrum 67(6):2351
185. Chen CA, Acquaviva P, Chun JH, Ando T (1996a) Scripta Materialia 34(5):689
186. Driesel W, Dietzsch Ch, Möser M (1996) J Phys D: Appl Phys 29:2492
187. Vieu C, Gierak J, David C, Lagadec Y, Bourlange A, Larigaldie D, Wang Z, Flicstein J, Launois H (1997) Microelectr Eng 35:349
188. Saito Y, Murata K, Hamaguchi K, Fujita H, Kotake S, Suzuki Y, Senoo M, Hu C-W, Kasuya A, Nishina Y (1998) J Cluster Sci 9(2):123
189. Sazio PJA, Vijendran S, Yu W, Beere HE, Jones GAC, Linfield EH, Ritchie DA (1999) J Crystal Growth 201/202:12
190. Vijendran S, Sazio PJA, Beere HE, Jones GAC, Ritchie DA, Norman CE (1999) J Vacuum Sci Technol B 17(6):3226
191. Akhmadaliev C, Mair GLR, Aidinis CJ, Bischoff L (2002) J Phys D: Appl Phys 35:L91
192. Akhmadaliev Ch, Bischoff L, Mair GLR, Aidinis CJ, Ganetsos Th, Anagnostakis E (2003) J Phys D: Appl Phys 36:L18
193. Akhmadaliev Ch, Bischoff L, Mair GLR, Aidinis CJ, Ganetsos Th (2004) Microelectr Eng 73–74:120
194. Mair GLR, Akhmadaliev Ch, Bischoff L, Ganetsos Th, Aidinis CJ (2003) Nuclear Instrum Meth Phys Res B 211:556
195. Mair GLR, Akhmadaliev Ch, Bischoff L, Ganetsos Th, Aidinis CJ, Anagnostakis EA (2004) Nucl Instrum Meth Phys Res B 217:347
196. Bischoff L, Mair GLR, Aidinis CJ, Londos CA, Akhmadaliev C, Ganetsos Th (2004c) Ultramicroscopy 100:1
197. Vijendran S, Lin SD, Jones GAC (2004) Microelectr Eng 73–74:111
198. Hu CW, Kasuya A, Wowro A, Horiguchi N, Czajka R, Nishina Y, Saito Y, Fujita H (1996) Mater Sci Eng A 217–218:103
199. Vijendran S, Jones GAC, Beere HE, Shields AJ (2000) Microelectr Eng 53:631
200. Krohn VE Jr (1961) In: Langmuir DB, Stuhlinger E, Sellen JM Jr (eds) Electrostatic propulsion. Academic Press, New York, London, pp 73–80
201. Mair GLR (1984) J Phys D: Appl Phys 17(11):2323
202. Beckman JC, Chang THP, Wagner A, Pease RFW (1996) J Vacuum Sci Technol B14(6):3911
203. Beckman JC, Chang THP, Wagner A, Pease RFW (1997) J Vacuum Sci Technol B15(6):2332
204. Aidinis CJ, Mair GLR, Bischoff L, Papadopoulos I (2001) J Phys D: Appl Phys 34:L14
205. Suvorov VG, Forbes RG (2004) Microelectr Eng 73–74:126
206. Mair GLR (1996) J Phys D: Appl Phys 29:2186
207. Gabovich MD (1983) Usp Fiz Nauk 140(1):137 (in Russian)
208. Gabovich MD, Poritsky WJa (1983) Zh Eksper Teor Fiz 85(1):146 (in Russian)
209. Praprotnik B, Driesel W, Dietzsch Ch, Niedrig H (1994) Surface Sci 314:353
210. Driesel W, Dietzsch Ch (1996) Appl Surface Sci 96:179
211. Bischoff L, Mair GLR, Mair AWR, Ganetsos T, Akhmadaliev C (2004b) Methods Phys Res B 222:622
212. Mair GLR (1990) J Phys D: Appl Phys 23:1239
213. Hesse E, Mair GLR, Bischoff L, Teichert J (1996) J Phys D Appl Phys 29:2193
214. Mair GLR, von Engel A (1979) J Appl Phys 50(9):5592
215. Thompson SP (1984) Vacuum 34(1–2):223
216. Barr DL (1987) J Vac Sci Technol B5(1):184
217. Kingham DR (1983) Appl Phys A 31(3):161
218. Mair GLR, Ganetsos Th, Bischoff L, Teichert J (2000) J Phys D: Appl Phys 33:L86
219. Swanson LW, Kingham DR (1986) Appl Phys A 41(3):223
220. Kingham DR, Swanson LW (1984) Appl Phys A 34(2):123
221. Kingham DR, Swanson LW (1986) Appl Phys A 41(2):157
222. Ganetsos Th, Mair GLR, Bischoff L, Teichert J, Kioussis D (2001) Solid State Electron 45:1049
223. Bischoff L, Teichert J, Ganetsos Th, Mair GLR (2001) J Vacuum Sci Technol B19(1):76
224. Aidinis CJ, Bischoff L, Mair GLR, Londos CA, Ganetsos Th, Akhamdaliev C (2004a) Microelectr Eng 73–74:116
225. Aidinis CJ, Mair GLR, Bischoff L, Londos CA, Akhamdaliev Ch, Ganetsos Th (2004b) Nuclear Instrum Meth Phys Res B 222:627
226. Gopalakrishnan MV, Metzgar K, Rosetta D, Krishnamurthy R (2003) J Mater Proc Technol 135:228
227. Yu F, Cui J, Ranganathan S, Dwarakadasa ES (2001) Mater Sci Eng A304–306:621
228. Lawley A, Leatham AG (1999) Adv Powder Technol, Mater Sci Forum 299(3):407
229. Chaudhury SK, Sivaramakrishnan CS, Panigrahi SC (2004) J Mater Proc Technol 145:385
230. Mesquita RA, Barbosa CA (2004) Mater Sci Eng A 383:87
231. Cantor B, Baik KH, Grant PS (1997) Progress Mater Sci 42:373
232. Smallman RE, Harris IR, Duggan MA (1997) J Mater Proc Technol 63:18
233. Schneider A, Uhlenwinkel V, Harig H, Bauckhage K (2004) Mater Sci Eng A 383:114
234. Srivastava VC, Mandal RK, Ojha SN (2001) Mater Sci Eng A304–306:555
235. Jayasinghe SN, Edirisinghe MJ (2005b) Appl Phys A 80:701
236. Valaskovic GA, Murphy III JP, Lee MS (2004) J Am Soc Mass Spectrom 15:1201